

Response to Referee number 1

8th December 2020

The authors would like to thank Referee no. 1 very much for his/her expertise and valuable comments to further improve and clarify the MS. We also appreciate his/her quick reaction. We have considered all recommendations and made the appropriate alterations. We also accomplished some other smaller corrections. Our specific responses are as follows, while the textual modifications amended can be traced in the marked-up version of the MS, which is attached.

Minor comments

L29. I am not sure what is meant here. Did you intend to refer to “the possible role of atmospheric vehicle-induced mixing processes”?

1. The sentence in Abstract was shortened by removing its unclear part.

L208: This unit conversion is based on the Magnus-equation.

2. The description of the conversion method was clarified by several, smaller textual modifications. See also Answer no. 3.

L210: The coefficients of this Magnus-equation can only be applied above liquid water. Different coefficients A and B are needed above ice surfaces, i.e. $T < 0$ °C.

3. Equation 1 with identical coefficients is acceptable for sub-cooled liquid water as well. We explicitly indicated in the text now that we utilized this approximation. The lowest 1-h mean T was ca. -5 °C, which confirms that this seems to be a plausible approach since the two saturation vapour pressure curves for liquid water and ice surface follow each other closely in the related temperature range. Moreover, the freezing occurred from January to the beginning of April, and, therefore, the conversion did not affect the restriction phases which were in the focus of the study.

L278: Before, in the methods section you stated that you report absolute humidity and you report values for relative humidity.

4. We performed the conversion of RH to AH in order to facilitate future comparison with other locations or cities in the world mainly for possible virology purposes. This conversion

requires the T data, and, therefore, the reader cannot accomplish it. For the objectives of the present study, however, the RH seems to be more relevant than AH and, therefore, we kept discussing the original property. The sentence explaining the purpose for the conversion was amended accordingly.

Figure 7: Could you please show this plot also for vehicle circulations, which would help to explain the observed differences in air pollutant concentrations.

5. The diurnal variations of vehicle circulation for all pandemic phases were shown Fig. S5 in the Supplement. On the request of the Referee, we extended now Fig. 7 by the panel showing the relevant vehicle circulation curves in the restriction phase, and added some further explanations. In addition, we emphasized better now in a proper place in the text that the corresponding plots can be find in the Supplement.

Figure 8 and 9: Please state that these plots show reanalysis data in the figure caption, so that the figure can be understood by itself.

6. The required extension was added to the figure captions.

L834: Is the expression in brackets really necessary?

7. The expression in brackets was deleted.

L855-L857: It is not clear to me what is meant by this sentence and how this conclusion is supported by the presented results.

8. The sentence indicated was removed from the MS.

Imre Salma
corresponding author

Response to Referee number 2

8th December 2020

The authors would like to thank Referee no. 2 very much for his/her expertise and valuable comments to further improve and clarify the MS. We have considered all recommendations and made the appropriate alterations. We also accomplished some other smaller corrections. Our specific responses are as follows, while the textual modifications amended can be followed in the marked-up version of the MS, which is attached.

1. Line 261-269: in this paragraph, the authors stated that the concentration of chemical species was based on the reanalyzed results of seven state-of-the-art European models. Please provide more descriptions about these models. If the reanalyzed data are publicly accessible, please provide a statement on how the data can be accessed.

Further details of the CAMS modelling method utilized were summarized and provided with a reference for the on-line availability of the model.

2. In section 3.1, the alterations in the T, RH, AH, WS, GRad and PBLHmax in the average reference year and year 2020 during the COVID-19 pandemic are quantified separately. How about the changes of wind direction? Previous studies indicated that a structure of convergence and divergence from the surface to the middle level of the troposphere also plays an important role in air pollution, so how about the convergence and divergence in the vertical direction over Budapest during the COVID-19 pandemic? The following paper is recommended for the discussion: Wu, J., Bei, N., Hu, B., Liu, S., Zhou, M., Wang, Q., Li, X., Liu, L., Feng, T., Liu, Z., Wang, Y., Cao, J., Tie, X., Wang, J., Molina, L. T., and Li, G.: Aerosol–radiation feedback deteriorates the wintertime haze in the North China Plain, *Atmos. Chem. Phys.*, 19, 8703–8719, <https://doi.org/10.5194/acp-19-8703-2019>, 2019.

We demonstrated earlier that the local wind direction (WD) at the BpART Laboratory is strongly modified by the built urban environment and local orography with respect to the synoptic wind (Salma et al.: Measurement, growth types and shrinkage of newly formed aerosol particles at an urban research platform, *Atmos. Chem. Phys.*, 16, 7837–7851, 2016, Sect. 3.2 and Fig. 5). This is the reason why we did not investigate directly the variations in WD. The long-range transport of air masses was, however, involved in the study through the macrocirculation patterns determined specifically for the geographical area. As far as the convergence and divergence in the vertical direction (as we understand, in the change of the vertical wind velocity) over Budapest is concerned, it does not seem to be substantially influence the air quality in the city

because of limitations constrained by the actual geographical location. We are aware that the vertical wind distribution could be connected e.g. to the heat island intensity, which is implicitly contained in the PBLH, and this latter quantity was indeed involved in the evaluations. The feedback mechanism discussed in the mentioned article is not relevant for us because 1) it occurs outside the COVID-19 time interval, and 2) the poor air quality in Budapest is usually associated with long-term cold air pool above the Carpathian Basin in winter, but it is accompanied by foggy situations and low radiation instead of wintertime haze, which is typical for the North China Plain. We would like to thank you very much for this comment because it triggered us to add a new section 3.8 Potentials as a follow up of this remark, where we could explain in more detail all this and the role of the T inversions for air quality issues in the Carpathian Basin in wintertime.

3. In Table S2, the median of hourly mean GRad in 2020 is less than that in the average reference year, and the lower radiation could suppress the development of the PBL, but the PBLH_{max} in 2020 is higher than that in the average reference year. Please provide explanation for this phenomenon.

The median GRad data (for $\geq 50 \text{ W m}^{-2}$) was lower in Y2020 by ca. 2.5 % than in Y3Ref, while the median PBLH_{max} value was larger in Y2020 by 10 % than in Y3Ref. We think that the two differences are insignificant when comparing them to the uncertainty intervals (in particular, for the modelled PBLH_{max}) and when considering the effects of some other confounding meteorological variables such as precipitation. We would not draw any conclusion on the relationships of GRad and PBLH_{max} based on such small differences. A short sentence dealing with this was added to the text to avoid any misunderstanding.

4. Line 277-280: Please provide quantitative results or references to explain why Spring 2020 is the third driest season since 1901.

The extremely dry spring in 2020 can likely be related to multifactorial meteorological reasons. Between 14 March and 24 April, anti-cyclonic weather types prevailed in the Carpathian Basin almost continuously for 41 days (Table S2). After this interval, the weather type was mostly cyclonic but with northerly wind, which brings dry and cold air masses into the Budapest area. These factors together resulted in the drought experienced. This was also briefly added to the MS.

5. Figure 8 and 9: In the figure caption, please clarify whether the data used are observations or simulations.

The captions of the figures were extended to include the requested information.

Imre Salma
corresponding author

1 What can we learn about urban air quality 2 with regard to the first outbreak of the COVID-19 pandemic? 3 A case study from Central Europe

4 Imre SALMA¹, Máté VÖRÖSMARTY¹, András Zénó GYÖNGYÖSI¹, Wanda THÉN²,
5 Tamás WEIDINGER³

6 ¹ Institute of Chemistry, Eötvös University, Budapest, Hungary

7 ² Hevesy György Ph. D. School of Chemistry, Eötvös University, Budapest, Hungary

8 ³ Department of Meteorology, Eötvös University, Budapest, Hungary

9 Correspondence to: Imre Salma (salma@chem.elte.hu)

10 **Abstract.** Motor vehicle road traffic in central Budapest was reduced by approximately 50 %
11 of its ordinary level for several weeks as a consequence of various limitation measures
12 introduced to mitigate the first outbreak of the COVID-19 pandemic in 2020. The situation was
13 utilised to assess the real potentials of urban traffic on air quality. Concentrations of NO, NO₂,
14 CO, O₃, SO₂ and particulate matter (PM) mass, which are ordinarily monitored in cities for air
15 quality considerations, aerosol particle number size distributions, which are not rarely
16 measured continuously on longer run for research purposes and meteorological properties
17 usually available were collected and jointly evaluated in different pandemic phases. The largest
18 changes occurred over the severest limitations (partial lock-down in the Restriction phase from
19 28 March to 17 May 2020). Concentrations of NO, NO₂, CO, total particle number (N_{6-1000})
20 and particles with a diameter <100 nm declined by 68, 46, 27, 24 and 28 %, respectively in
21 2020 with respect to the average reference year of 2017–2019. Their quantification was based
22 on both relative difference and standardised anomaly. The change rates expressed as relative
23 concentration difference due to relative reduction in traffic intensity for NO, NO₂, N_{6-1000} and
24 CO were 0.63, 0.57, 0.40 and 0.22 (%/%), respectively. **Of the pollutants which reacted in a
25 most sensitive manner to the change in vehicle circulation, it is the NO₂ that shows the most
26 frequent exceedance of health limits. Intentional tranquillizing of the vehicle flow has
27 considerable potentials in improving the air quality. At the same time, the concentration levels
28 of PM₁₀ mass, which is the most critical pollutant in many European cities including Budapest,
29 did not seem to be largely affected by vehicles. Concentrations of O₃ concurrently showed an
30 increasing tendency with lower traffic, which was explained by its complex reaction
31 mechanism. Modelling calculations indicated that spatial gradients of NO and NO₂ within the
32 city became further enhanced by reduced vehicle flow, ~~which indicates the possible role of
33 atmospheric processes taking place in near-city background environments.~~**

34 **1 Introduction**

35 The coronavirus disease (COVID-19) is caused by the novel, Severe Acute Respiratory
36 Syndrome CoronaVirus 2 (SARS-CoV-2) virus. The outbreak was declared as a pandemic by
37 the WHO on 11 March 2020 (WHO, 2020). National governments, international agencies and
38 organisations enacted widespread emergency actions for individuals, some professionals,
39 communities and the public to reduce the risk of infection and to combat the plague. As a
40 consequence of the implemented measures, road traffic in many cities worldwide was reduced
41 in a substantial manner and for a considerable time interval. In parallel, lower concentrations
42 of several air pollutants were reported from both satellite observations and in situ
43 measurements (Keller et al., 2020; Lal et al., 2020; Le et al., 2020; Lee et al. 2020; Mahato et
44 al., 2020; Nakada and Urban, 2020; Petetin et al., 2020; Tobías et al., 2020; Wang et al., 2020).

45
46 This situation offers a unique possibility for atmospheric scientists to investigate
47 experimentally some important atmospheric chemical and physical issues including urban air
48 quality and climate change under extraordinary conditions of lower traffic and industrial
49 productivity (Sussmann and Rettinger, 2020). The results and consequences of this real
50 “ambient experiment” can be utilised to determine the true potentials of action plans on
51 tranquillizing urban road circulation for handling air quality, overcrowding, traffic congestions,
52 noise contamination and other environmental, health and climate impacts in large cities.

53
54 The task is, however, somewhat complicated. Actual concentrations of atmospheric
55 constituents can depend on 1) their emissions from several sectors, 2) their physical removal
56 processes, 3) local meteorological conditions mainly precipitation (P), wind speed (WS),
57 planetary boundary layer height (PBLH) and atmospheric stability, 4) their (long-range)
58 transport and 5) possible photochemical reactions, which are largely influenced by other
59 meteorological properties such as global solar radiation (G_{Rad}), relative humidity (RH) and
60 air temperature (T), and by availability of and interactions with other chemical species present
61 in the air. Many of the phenomena or properties listed are, in addition, interconnected and
62 confound, which further obscures the situation since they create an internally interacting
63 environmental system.

64
65 Tropospheric residence time of constituents can also play a role under non-steady-state
66 conditions (Harrison, 2018). As a result, atmospheric concentrations at a fixed site change both

67 periodically and randomly (fluctuate) on daily, seasonal or annual scales. The variations are
68 also linked to the geographical location and features of urban sites (de Jesus et al., 2019).

69

70 Source-specific markers generated by internal combustion engines or added on purpose into
71 their fuel (e.g. Horvath et al., 1988; Gentner et al., 2017) or multivariate statistical methods
72 (Hopke, 2016) can be applied to estimate the importance of vehicle traffic for air quality. These
73 methods usually require advanced analytical methods to obtain data for specific species, which
74 may not be available with a required time resolution, or need a larger number of data, which
75 can be constrained by duration of the time intervals of interest. Another possibility is to
76 examine jointly the time series of multicomponent atmospheric data sets. This approach
77 (described later in more detail) can be utilised retrospectively and it is generally applicable in
78 different cities in the world, which were affected by road traffic restrictions.

79

80 In Hungary, state of emergency was introduced on 11 March 2020. It involved sequential
81 closure of education institutes, beginning of work-from-home and social distancing. It was
82 followed by restrictions on movement. During this, residences could only be left with specified
83 basic purposes, administrative centres, restaurants and touristic places were closed, distant
84 travels were ceased, public parks were closed for long weekends and there were various time
85 limitations on shopping. The mitigating measures resulted in perceivable changes in vehicular
86 road traffic and atmospheric concentrations. The main objectives of the present paper are 1) to
87 introduce and demonstrate a general method for quantifying concentration changes, 2) to
88 evaluate whether the changes observed were related to motor vehicle road traffic, 3) to assess
89 the effect of traffic on these alterations, and 4) to estimate and debate the potentials of
90 tranquillized urban vehicle flow on the air quality.

91 **2 Methods**

92 Criteria air pollutants, namely NO, NO₂=NO_x-NO, CO, O₃, SO₂ and particulate matter (PM)
93 mass in various size fractions were involved in the study. The species originate from different
94 sources. Vehicular road traffic is usually associated with NO and CO, while NO₂ and O₃ are
95 formed by chemical reactions in the air. Contributions of residential heating, cooking, industrial
96 activities, regional traffic in winter and secondary processes to PM_{2.5} mass are of large
97 importance in many cities, including Budapest. At the same time, PM₁₀ mass represents
98 disintegration sources, e.g. windblown soil, crustal rock, mineral and roadside dust,

99 resuspended dust by car movement, agricultural activities in the region, construction work and
100 material wear such as tire abrasion of cars at kerbside sites (Salma and Maenhaut, 2006; Putaud
101 et al., 2010; Harrison et al., 2012; Salma et al., 2020a). They all can be important particularly
102 under dry weather conditions.

103

104 Aerosol particle number concentrations in the diameter ranges from 6 to 1000 nm (N_{6-1000}) and
105 from 6 to 100 nm (N_{6-100}) are mainly assigned to high-temperature emission sources (such as
106 vehicle road traffic or incomplete burning) and atmospheric new particle formation and growth
107 (NPF) events (Paasonen et al., 2016; Rönkkö et al., 2017; Salma et al., 2017). The latter process
108 occurs as a daily phenomenon with a typical shape of its monthly occurrence frequency (Salma
109 and Németh, 2019). This distribution changes in Budapest from year to year without any
110 tendentious character (Salma et al., 2020b). Particles with a diameter from 25 to 100 nm (N_{25-}
111 $_{100}$) in cities are mainly emitted by incomplete combustion or consist of grown new particles
112 by condensation, while the size fraction with a diameter from 100 to 1000 nm ($N_{100-1000}$)
113 expresses physically and chemically aged particles, thus, they represent larger spatial extents
114 (Salma et al., 2014; Mikkonen et al., 2020).

115

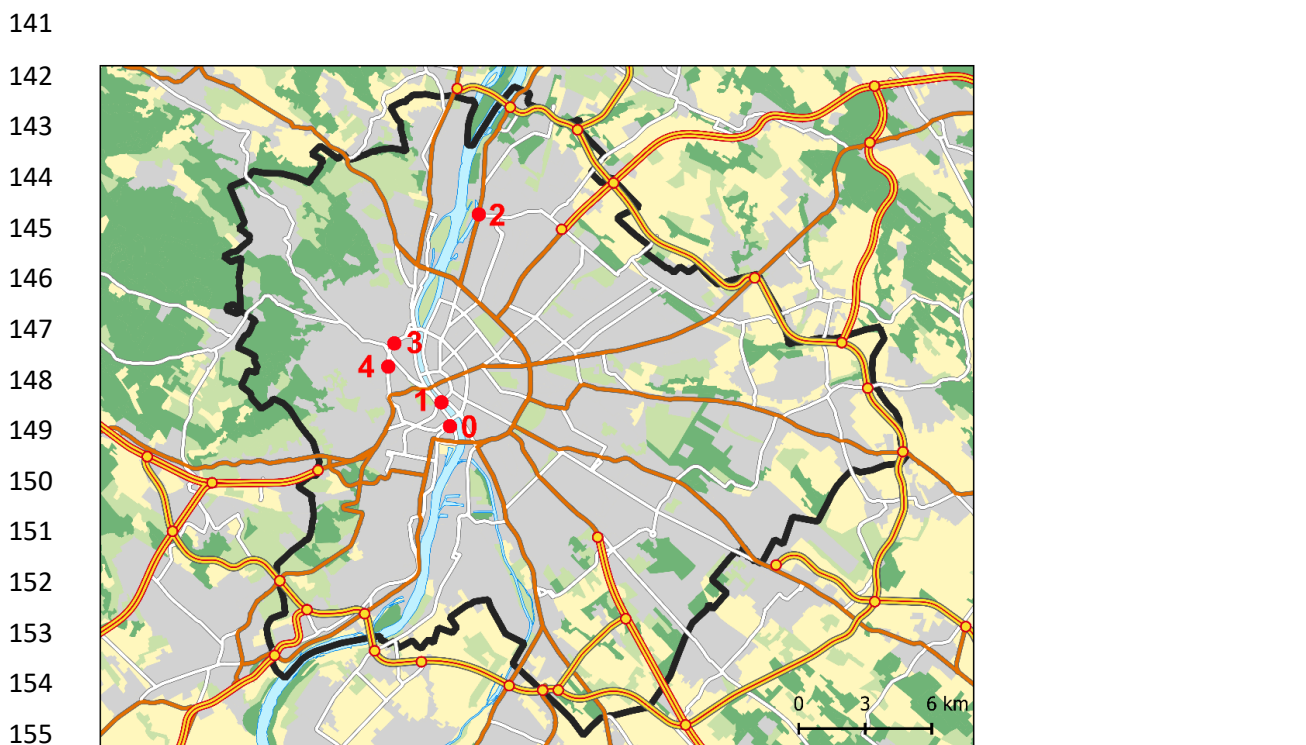
116 Approximate tropospheric residence time of NO_x , CO, O_3 , SO_2 and PM are estimated to 1–2
117 days, 2 months, 1–2 months, 4–12 days and from several hours up to 1 week depending largely
118 on particle size and chemical composition, respectively (Warneck and Williams, 2012;
119 Harrison, 2018).

120 **2.1 Experimental data**

121 The concentrations of NO/NO_x , CO, O_3 , SO_2 , PM_{10} mass and $\text{PM}_{2.5}$ mass were measured by
122 chemiluminescence (Thermo 42C), IR absorption (Thermo 48i), UV fluorescence (Ysselbach
123 43C), UV absorption (Ysselbach 49C) and beta-ray attenuation (two Environment MP101M
124 instruments with PM_{10} and $\text{PM}_{2.5}$ inlets) methods, respectively with a time resolution of 1 h.
125 **The concentrations of gases were expressed at a temperature of 293 K and pressure of 101.3**
126 **kPa.** The particle number concentrations were determined by a flow-switching type differential
127 mobility particle sizer (DMPS; Salma et al., 2016b) with a time resolution of 8 min. The latter
128 measurements were performed in a diameter range from 6 to 1000 nm in 30 size channels with
129 equal width in the dry state of particles. The meteorological data of T , RH and WS and of GRad

130 were measured by standardised sensors (HD52.3D17, Delta OHM, Italy, and SMP3
131 pyranometer, Kipp and Zonen, the Netherlands, respectively) with a time resolution of 1 min.

132
133 The DMPS and meteorological measurements were accomplished at the Budapest platform for
134 Aerosol Research and Training (BpART) Laboratory (N 47° 28' 29.9", E 19° 3' 44.6", 115 m
135 above mean sea level) of the Eötvös University (Fig. 1). The location represents a well-mixed,
136 average atmospheric environment for the city centre due to its geographical and meteorological
137 conditions (Salma et al., 2016a). The local emissions include diffuse urban traffic exhaust,
138 household/residential emissions and limited industrial sources together with some off-road
139 transport (Salma et al., 2020a). In some time intervals, long-range transport of air masses can
140 also play a role.



156 **Figure 1.** Location of the measurement sites in Budapest. 0: BpART Laboratory, 1: Szabadság Bridge,
157 2: Váci Road, 3: Széna Square and 4: Alkotás Road. The border of the city (in black colour), Danube
158 River and the major routes are also indicated.

159
160 The data of the criteria air pollutants were acquired from a measurement station of the National
161 Air Quality Network at Széna Square (Fig. 1) located in 4.5 km from the BpART Laboratory
162 in the upwind-prevailing direction (Salma and Németh, 2019). This station serves as a reference
163 for our long-term air quality-related research activities in several aspects and proved to be
164 acceptable for this purpose.

165

166 Atmospheric transport of chemical species was assessed through large-scale weather types. We
167 utilised macrocirculation patterns (MCPs), which were invented specifically for the Carpathian
168 Basin (Péczely, 1957; Maheras et al., 2018). The classification of the MCPs is based on the
169 position, extension and development of cyclones and anticyclones relative to the Carpathian
170 Basin considering the sea-level pressure maps constructed for 00:00 UTC in the North-
171 Atlantic–European region on a daily basis. A brief survey on the MCPs and the actual codes
172 for year 2020 utilised in the interpretations are given in Table S1 and Fig. S1, respectively in
173 the Supplement. The relative occurrences of the weather types in year 2020 were roughly in
174 line with multiple-year frequencies. Extended anticyclonic weather types usually indicate that
175 the air masses are stagnant, and that the importance of local or regional sources prevail over
176 the air transport from distant sources. Under cyclonic weather conditions and frontal systems,
177 the transported air masses can yield more pronounced effects and contributions.

178

179 Census of motor road vehicles was performed on three major routes and on a bridge over the
180 Danube River by the Budapest Public Roads Ltd. The measurement sites were on Szabadság
181 Bridge, Váci Road, around Széna Square and Alkotás Road (Fig. 1), which are described in
182 more detail in the Supplement. The counting was based on permanent electronic devices with
183 inductive loops and passenger cars, high- and heavy-duty vehicles and buses were recorded in
184 both directions. The time resolution of the data was 1 h and their coverage was >90 % of all
185 possible item in a year. The sites cover a wide range of maximum hourly mean vehicle flow
186 from about 1200 to 4600 h⁻¹. Szabadság Bridge has the smallest traffic intensity of the sites,
187 but it proved to be a very valuable microenvironment for the study since it is part of the internal
188 boulevard. The routes showed coherent and common aggregate time properties and, therefore,
189 their data are to be proportional to general vehicular traffic flow in the city centre.

190 **2.2 Time intervals of interest**

191 Time intervals from 1 January to 31 July in 2017, 2018, 2019 and 2020 were studied. This
192 included all major measures related to the first outbreak of the Covid-19 pandemic in Budapest
193 in 2020. Within these seven months, five consecutive time intervals were selected for
194 comparative purposes: 1) from 1 January till the beginning of the state of emergency at 15:00
195 on 11 March, which is referred as Pre-emergency phase, 2) from the beginning of the state of
196 emergency to 27 March (till the beginning of the restriction on movement), which is called

197 here Pre-restriction phase, 3) from the beginning of the restriction on movement till its end in
198 Budapest on 17 May, which is denoted as Restriction phase, 4) from the end of the restriction
199 on movement in Budapest till the end of the state of emergency on 17 June, which is referred
200 as Post-restriction phase and 5) from the end of the state of emergency till 31 July, which is
201 called Post-emergency phase. An overview on the pandemic phases with further details of
202 possible relevance for air quality issues is summarised in Fig. S1. Equivalent time intervals in
203 years 2017–2019, which correspond to these phases were considered for comparative purposes.

204
205 Local daylight saving time (LDST=UTC+1 or UTC+2) was chosen as the time base for the
206 atmospheric concentrations and road traffic data because it was observed that the daily activity
207 time patterns of inhabitants largely influences these variables in cities (Salma et al., 2014). The
208 meteorological data were expressed in UTC+1 since their diurnal and seasonal behaviours are
209 primarily controlled by sun path and other natural processes.

210 2.3 Data treatment and modelling

211 Medical studies with the influenza virus indicated that absolute humidity (AH) constrains both
212 transmission efficiency and virus survival more than RH (Shaman and Kohn, 2009). ~~For this~~
213 ~~reason, In order to facilitate the future comparison with other locations or cities in the world~~
214 ~~mainly for possible virology purposes,~~ the hourly mean RH values (%) were converted to AH
215 (g m⁻³) ~~by a practical form of Clausius-Clapeyron equation using a calculation recommended~~
216 ~~by WMO (2008):~~

$$217$$
$$218 \text{AH} = \frac{e(T_0) \times \exp\left(A \times \frac{T}{T+B}\right) \times \text{RH} \times C}{T+273.15}, \quad (1)$$

219

220 where T is expressed in °C, $e(T_0)=6.112$ hPa is the saturation vapour pressure at $T_0=0$ °C,
221 $A=17.67$, $B=243.5$ °C and $C=2.167$ (WMO, 2008). ~~For air temperatures <0 °C, we used an~~
222 ~~approximation for sub-cooled liquid water and adopted identical coefficients. This seems to be~~
223 ~~a plausible approach since the saturation vapour pressure curves for liquid water and ice surface~~
224 ~~follow each other closely near the freezing point. The AH values are summarised in Table S2,~~
225 ~~while we keep evaluating the RH because it seems to be more relevant for the purpose of this~~
226 ~~atmospheric study than the former property.~~

227

228 Vertical transfer of gases and aerosol particles emitted or generated at the Earth surface can
229 largely be affected by the dynamics of the PBLH. It is realised by the dilution of pollutants
230 with mixing. The PBLH data were obtained from the 5th generation of the European Center of
231 Medium-Range Weather Forecasts (ECMWF) atmospheric reanalysis (ERA5) database using
232 Copernicus Climate Change Service (C3S, 2017). The ERA5 combines the modelled data of
233 the ECMWF's Integrated Forecast System, version CY41R2 on 137 hybrid sigma vertical
234 levels with newly available observations assimilated at every hour. In the present study, the
235 daily maximum PBLH values ($PBLH_{max}$) were considered to be proportional to the volume of
236 the mixed air parcel.

237

238 The data with a time resolution of smaller than 1 h were averaged for 1 h. The coverage of the
239 hourly data was typically above 90 % of all items in each year. Descriptive statistics, thus
240 count, minimum, median, maximum, geometric mean with standard deviation (SD) of all
241 variables were derived for the time interval studied and its each pandemic phase in year 2020
242 (Y2020). The characteristics were compared to the corresponding data in an average reference
243 year (Y3Ref). This contains averages of the parallel hourly mean data of the years 2017–2019.
244 Longer time span than three years would not necessarily be advantageous since some chemical
245 species in Budapest show tendentious change on a scale of ten years (Mikkonen et al., 2020)
246 and the urban traffic could also change substantially.

247

248 Comparative evaluations are often performed via the relative change (RDiff) of medians (m)
249 derived for a selected time span, which can be described as

250

$$251 \text{RDiff} = \frac{m(Y2020) - m(Y3Ref)}{m(Y3Ref)}. \quad (2)$$

252

253 In our case, the time spans considered were the intervals of the five pandemic phases in both
254 Y2020 and Y3Ref. The quantity RDiff essentially expresses the ratio of medians. It is very
255 important to stress immediately that the ratios are largely influenced by the absolute magnitude
256 of variables and could be misleading if interpreted alone. In addition, different variables can
257 have very different ranges of variability. A further metric that could, therefore, be involved is
258 the standardised anomaly (SAly), which is described as

259

$$260 \text{SAly} = \frac{m(Y2020) - m(Y3Ref)}{SD}. \quad (3)$$

261

262 This quantity expresses the observed differences in units of SD, so it brings out the relative
263 asset of the actual difference. For GRad, which evolves daily from their very low values
264 overnight in a large number, which were not considered, the anomaly was not standardised to
265 its (expanded) SD, but instead, it was calculated simply as a difference $m(Y2020)-m(Y3Ref)$
266 in its absolute unit.

267

268 A difference in the fluctuating and periodically varying data sets (see Sect. 1) over a pandemic
269 phase in Y2020 was quantified to be significant with respect to the equivalent interval in Y3Ref
270 if both their RDiff and SAly metrics were significant. The actual criteria adopted are specified
271 and discussed in Sect. 3.5.

272

273 Average diurnal variations of all variables for workdays and holidays over each pandemic
274 phase in the average reference year 2017–2019 and year 2020 were calculated by selecting all
275 individual data for a particular hour of day on workdays or on holidays over the time interval
276 under evaluation and by averaging them.

277

278 The spatial distributions of the chemical species of interest over the city during each pandemic
279 phase were modelled via the surface concentrations derived from the Copernicus Atmosphere
280 Monitoring Service (CAMS) with a grid resolution of $0.1^\circ \times 0.1^\circ$ in order to study their potential
281 differences (CAMS, 2019). The reanalysed concentrations are based on the following state-of-
282 the-art European models CHIMERE, EMEP, EURAD-IM, LOTOS-EUROS, MATCH,
283 MOCAGE and SILAM (Marécal et al., 2015). **The modelled concentrations are represented by
284 the CAMS ensemble, which is the median of the available model results at each grid-point.
285 The CAMS modelling shares the meteorological driver of the ECMWF's Integrated Forecast
286 System and the Monitoring Atmospheric Composition and Climate emission inventory of the
287 Netherlands Organization for Applied Scientific Research.** The system provides daily 96-h
288 estimates with hourly outputs of several chemical species. The hourly analysis at the Earth
289 surface is done a posteriori for the past day using a selection of air quality data from the
290 corresponding European monitoring stations.

291 **3 Results and discussion**

292 The changes in atmospheric concentrations are presented and interpreted after the effects of the
293 confound variability in local meteorological conditions and in (long-range) transport of
294 atmospheric air masses are evaluated and quantified.

295 **3.1 Meteorological conditions**

296 The hourly average meteorological data over the time interval considered were in line with
297 ordinary characteristics measured at the BpART Laboratory (Salma and Németh, 2019;
298 Mikkonen et al., 2020). The T in 2020 was colder by 0.4 °C than in the average reference year,
299 and the relative differences for median RH, WS, GRad and PBLH_{max} were -3, -8, +3 and +15
300 %, respectively. These alterations, except for the PBLH_{max}, are not significant (remained within
301 ±10 %). There were, however, two important alterations from the multiple-years' weather
302 situations. First, spring 2020 was extraordinary dry; it was the third driest season since 1901.
303 ~~This can likely be related to multifactorial meteorological reasons. The drought started after 7~~
304 ~~March and continued in April and May~~Between 14 March and 24 April, anti-cyclonic weather
305 types prevailed in the Carpathian Basin almost continuously for 41 days (Fig. S1). After this
306 interval, the weather type was mostly cyclonic but with northerly wind, which ordinary brings
307 dry and cold air masses to the Budapest area. These factors together resulted in long and severe
308 drought experienced. Finally, it was followed by frequent, continued and spatially extended
309 rains in June (Fig. S1). Secondly, the number of foggy hours (160) in January 2020 was more
310 than four times larger than in the average reference year. This conclusion is based on the
311 measurements at the Budapest Liszt Ferenc International Airport.

312
313 An overview on the major meteorological data during the whole state of emergency interval
314 (98 days) is summarised in Table S2. The drought did not seem to influence substantially the
315 WS and GRad but affected considerably the RH and indirectly the PBLH_{max}. The alterations in
316 the PBLH_{max} in the average reference year and year 2020 over the pandemic phases are,
317 therefore, quantified separately in Table 1 and are also displayed in Fig. S2. The time series for
318 WS and T are also given in Figs. S3 and S4, respectively. It is seen in Fig. S2 that the Restriction
319 phase – which is of particular interest for this study – was influenced by the PBLH_{max} in a
320 more-or-less persistent manner without larger oscillations or fluctuations. The RDiff properties
321 are taken into consideration when quantifying the concentration changes (Sect. 3.5). ~~Lastly, it~~
322 ~~should also be mentioned that some of the differences in the meteorological data become small~~

323 or insignificant when comparing them to their uncertainty intervals (in particular, for the
324 modelled $PBLH_{max}$).

325

326 **Table 1.** Medians of the daily maximum planetary boundary layer height (km) in the average reference
327 year of 2017–2019 (Y3Ref) and year 2020 (Y2020) together with their relative difference (RDiff) in %
328 and their anomaly standardised to SD (SAly) over the five consecutive phases of the first COVID-19
329 outbreak.

330

Pandemic phase	Y3Ref	Y2020	RDiff	SAly
Pre-emergency	0.66	0.88	+32	+0.4
Pre-restriction	1.4	1.4	+1	+0.0
Restriction	1.5	1.8	+18	+0.5
Post-restriction	1.6	1.3	-21	-0.7
Post-emergency	1.8	1.7	-8	-0.3

331

332 3.2 Motor vehicle road traffic

333 Time series of vehicle flow on a major route (Váci Road, site no. 2 in Fig. 1) over the time
334 interval studied in the average reference year and year 2020 are shown in Fig. 2 as examples.
335 The other urban sites exhibited very similar time behaviour and tendencies.

336

337 The time series for vehicle flow showed a clear periodicity. On each workday, two peaks –
338 corresponding to the early morning and late afternoon rush hours – can be identified. In addition
339 to this periodicity, the smoothed curves also revealed an obvious cycling due to repeated
340 workdays and holidays sequence. More importantly, the time series implied that in the Pre-
341 emergency pandemic phase, the road traffic in the city centre in Y2020 was very similar to that
342 in Y3Ref. The difference only appeared as a horizontal shift in time, which was caused by the
343 occurrence of holidays in the average reference year and year 2020. Two weeks before the
344 introduction of the restriction on movement, the vehicle circulation already started declining,
345 and in the last week of the Pre-restriction phase, it already reached the level observed later in
346 the Restriction phase. During these eight or nine weeks, the vehicular circulation on workdays
347 was around the ordinary levels on holidays in 2017–2019. The circulation approached its
348 ordinary values within or after the first week of the Post-restriction phase step wisely. After

349 that, the curves for the two years were at almost identical levels again. The changes in the
 350 vehicle flow are quantified in Sect. 3.5 together with the pollutant concentrations.

351

352

353

354

355

356

357

358

359

360

361

362

363

364

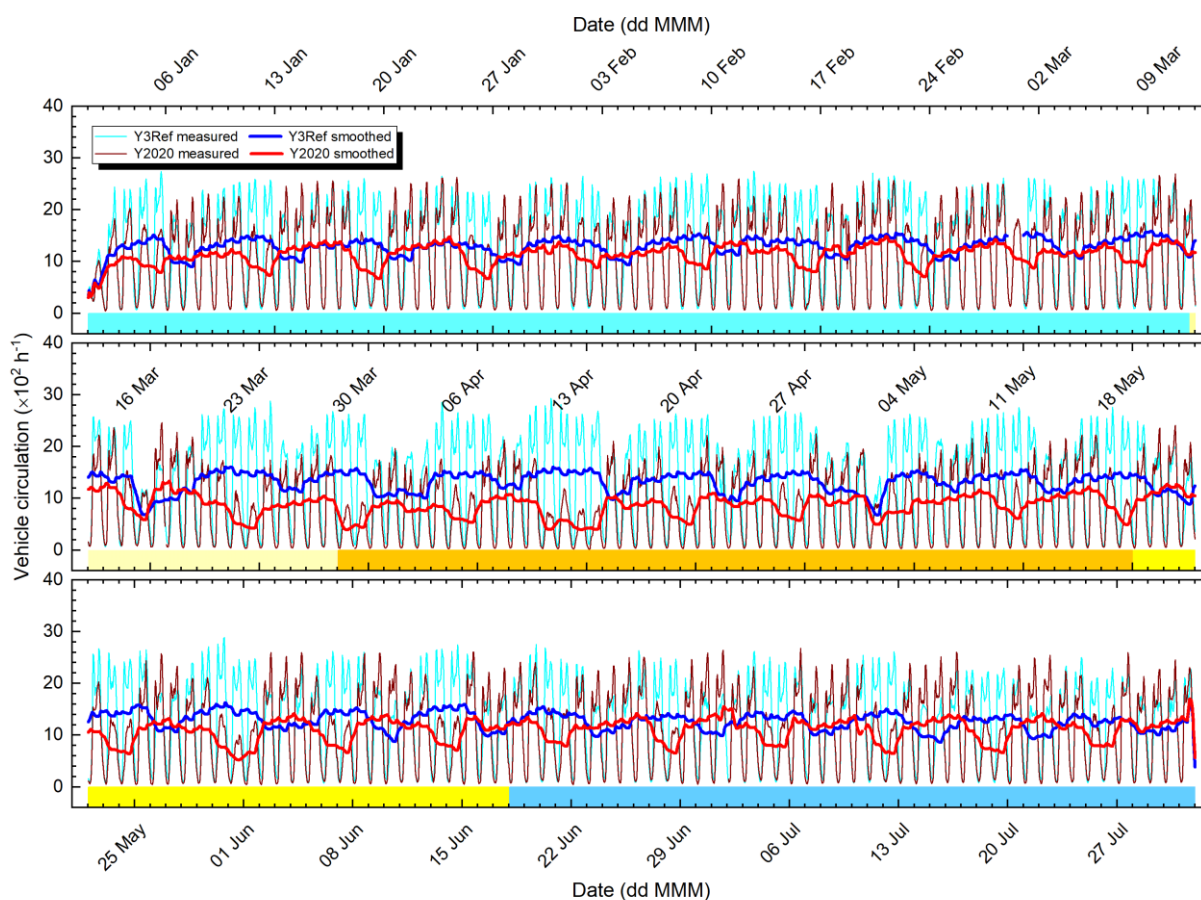
365

366

367

368

369



370 **Figure 2.** Time series of motor vehicle circulation on a major route (Váci Road) in Budapest in both
 371 directions in the average reference year of 2017–2019 (Y3Ref) and year 2020 together with their 24-h
 372 smoothed curves over the five consecutive phases of the first COVID-19 outbreak. The phases are
 373 marked by the following colour codes: Pre-emergency phase lighter blue, Pre-restriction phase lighter
 374 yellow, Restriction phase orange, Post-restriction phase darker yellow and Post-emergency phase
 375 darker blue. The tick labels of the abscissa indicate the Mondays in 2020.

376

377 The shapes of the diurnal patterns (Fig. S5) for the average reference year and year 2020 were
 378 similar to each other with some modifications. Differences could be identified in Pre-restriction
 379 and Restriction pandemic phases between 16:00 and 19:00, when the traffic flow on weekends
 380 seemed to be systematically and in excess lower in 2020 than in the average reference year.
 381 This could be due to the limitations on shopping and to modified going out routines of
 382 inhabitants under the restrictions. Similarly, the early morning peak on workdays in the Post-
 383 emergency (and partly in the Post-restriction) phases was smaller in excess in Y2020 than in
 384 Y3Ref, which can likely be linked to less people going physically to work due to propagated

385 home-office jobs. To facilitate the comparison of diurnal patterns of vehicle circulation and of
 386 atmospheric concentrations, the plot showing the diurnal variation of concentrations in the
 387 Restriction phase was extended by the vehicle flow in the same pandemic phase (Fig. 7).

388 3.3 Time series of concentrations

389 Time series of NO, O₃, PM_{2.5} mass and N₆₋₁₀₀₀ atmospheric concentrations over the time
 390 interval studied are shown in Figs. 3–6, respectively. The chemical species selected represent
 391 primary pollutant gases, secondary pollutant gases and two different aerosol properties,
 392 respectively. The corresponding curves for NO₂, CO, SO₂, PM₁₀ mass and N₁₀₀₋₁₀₀₀ are
 393 displayed in Figs. S6–S10, respectively.

394

395

396

397

398

399

400

401

402

403

404

405

406

407

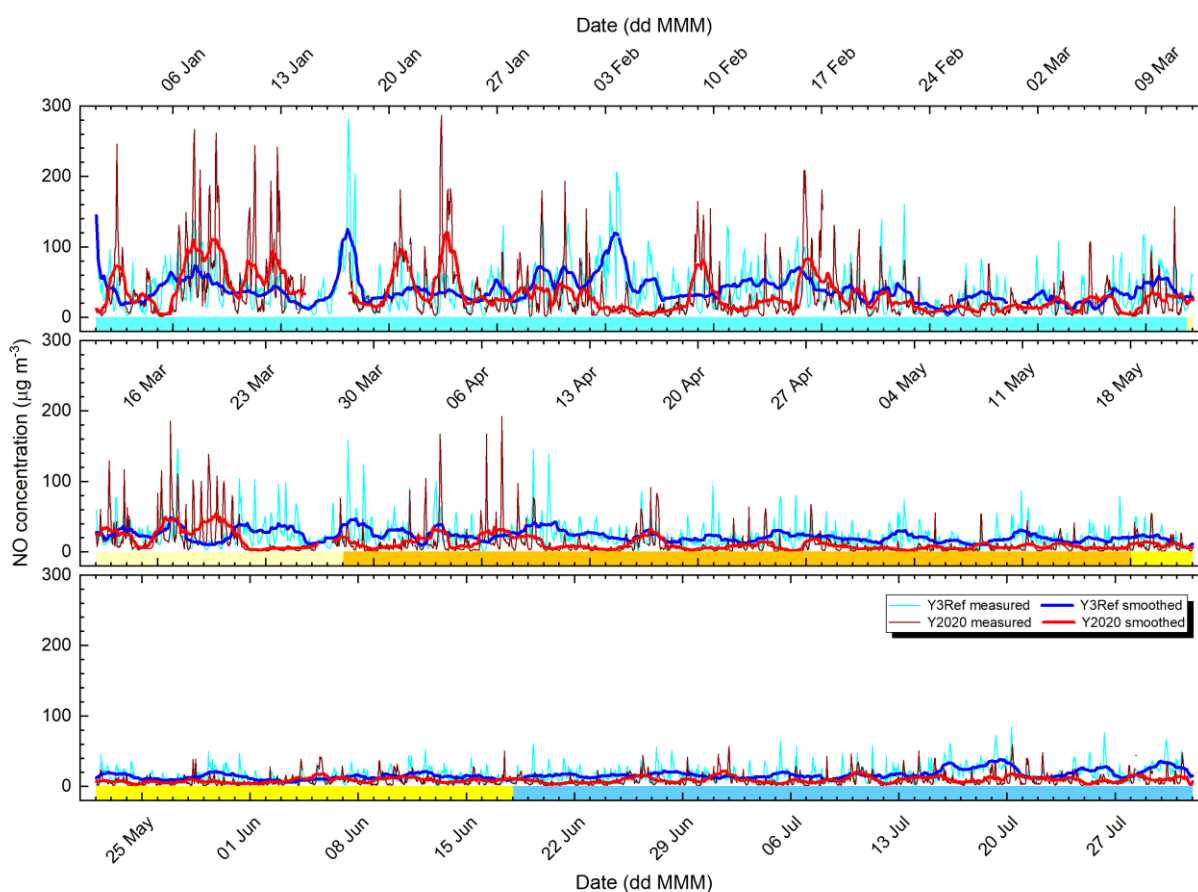
408

409

410

411

412



413 **Figure 3.** Time series of NO concentration in the average reference year of 2017–2019 (Y3Ref) and
 414 year 2020 together with their 24-h smoothed curves over the five consecutive phases of the first
 415 COVID-19 outbreak. The phases are marked by the following colour codes: Pre-emergency phase
 416 lighter blue, Pre-restriction phase lighter yellow, Restriction phase orange, Post-restriction phase darker
 417 yellow and Post-emergency phase darker blue. The tick labels of the abscissa indicate the Mondays in
 418 2020.

419

420 The curves for both measured and smoothed data demonstrated that the concentrations varied
421 substantially in time. The changes on the smoothed curves seemed to be fluctuations on a daily
422 scale and for some pollutants, they appeared to exhibit some tendencies on a monthly scale,
423 while the data series possessed diurnal periodicity as well. The trends, i.e. the smoothed curves
424 over the seven months are in line with the distributions of the monthly median concentrations
425 of the species at identical locations determined for several years (Salma et al., 2020b).

426

427

428

429

430

431

432

433

434

435

436

437

438

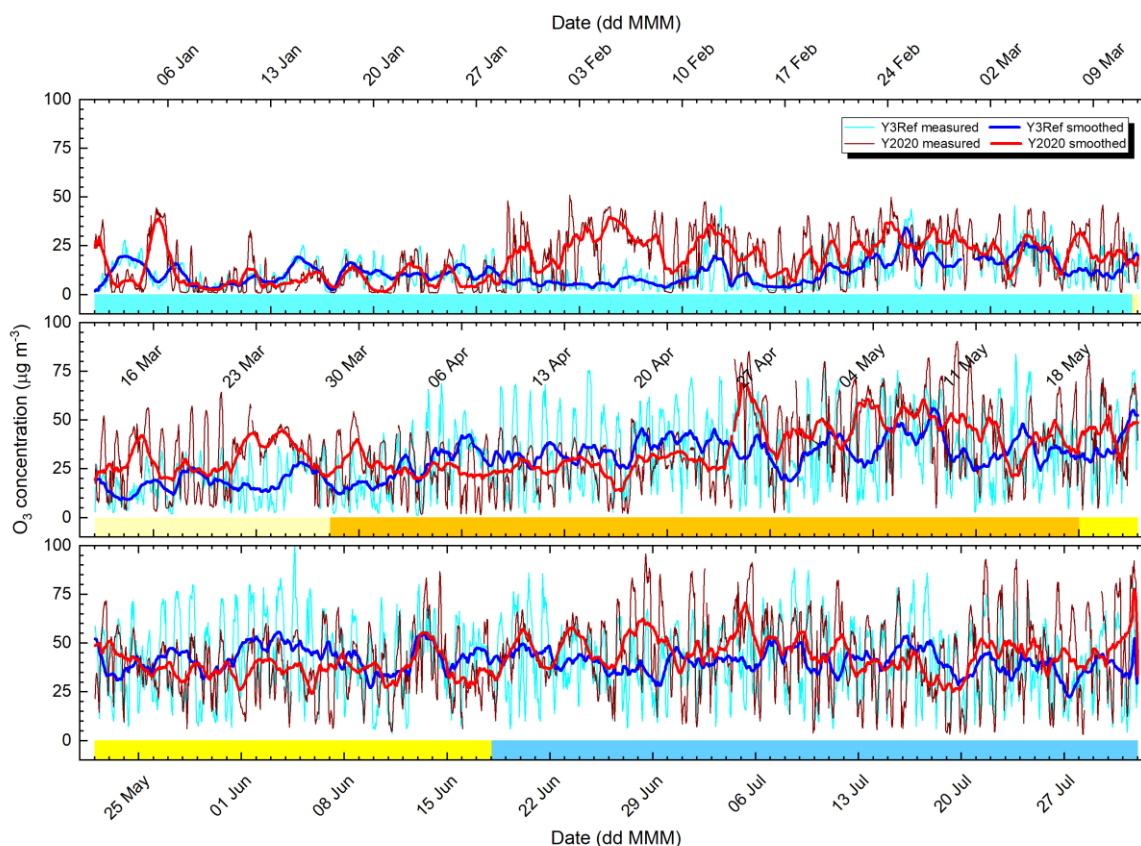
439

440

441

442

443



444 **Figure 4.** Time series of O₃ concentration in the average reference year of 2017–2019 (Y3Ref) and year
445 2020 together with their 24-h smoothed curves over the five consecutive phases of the first COVID-19
446 outbreak. The phases are marked by the following colour codes: Pre-emergency phase lighter blue, Pre-
447 restriction phase lighter yellow, Restriction phase orange, Post-restriction phase darker yellow and Post-
448 emergency phase darker blue. The tick labels of the abscissa indicate the Mondays in 2020.

449

450 The annual relative SDs (RSDs) for NO, NO₂, CO, O₃, SO₂, PM₁₀ mass, PM_{2.5} mass, N_{6–1000},
451 N_{6–100}, N_{25–100} and N_{100–1000} in years 2017–2019 were 115, 56, 43, 91, 37, 56, 74, 63, 69, 68 and
452 68 %, respectively (cf. Sect. 1). Their time distributions were complex. For species, which do
453 not normally show seasonal tendency such as particle number concentrations and perhaps PM₁₀

454 mass, the distributions of monthly RSDs were also featureless. For SO₂, which tends to exhibit
 455 smaller concentration levels in summer than in winter, the distribution of its monthly RSDs
 456 seemed to have an opposite behaviour. For O₃, which exhibits larger concentrations in summer
 457 than in winter, the distribution of monthly RSDs showed again an opposite behaviour. These
 458 relationships are in accordance with general metrological expectations. Excitingly, for NO,
 459 NO₂, CO and perhaps PM_{2.5} mass, the distributions of monthly RSDs appeared to roughly
 460 follow in parallel the concentration trends within the concentration ranges actually obtained.
 461 The largest decrease in the RSDs from winter to summer was observed for NO, which was
 462 approximately 20 % (of its annual mean RSD). The latter association could likely be linked to
 463 meteorological conditions and source/sink intensities of these pollutants.

464

465

466

467

468

469

470

471

472

473

474

475

476

477

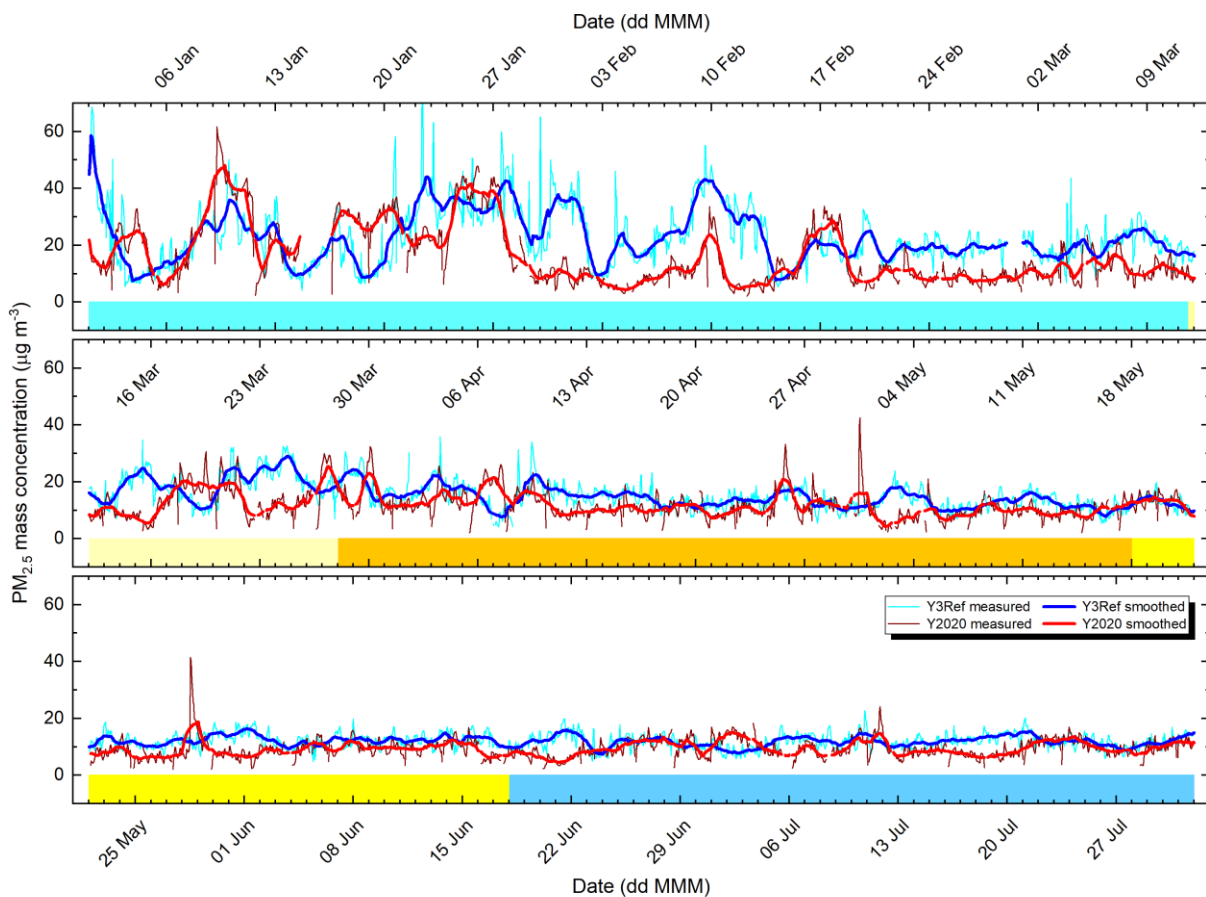
478

479

480

481

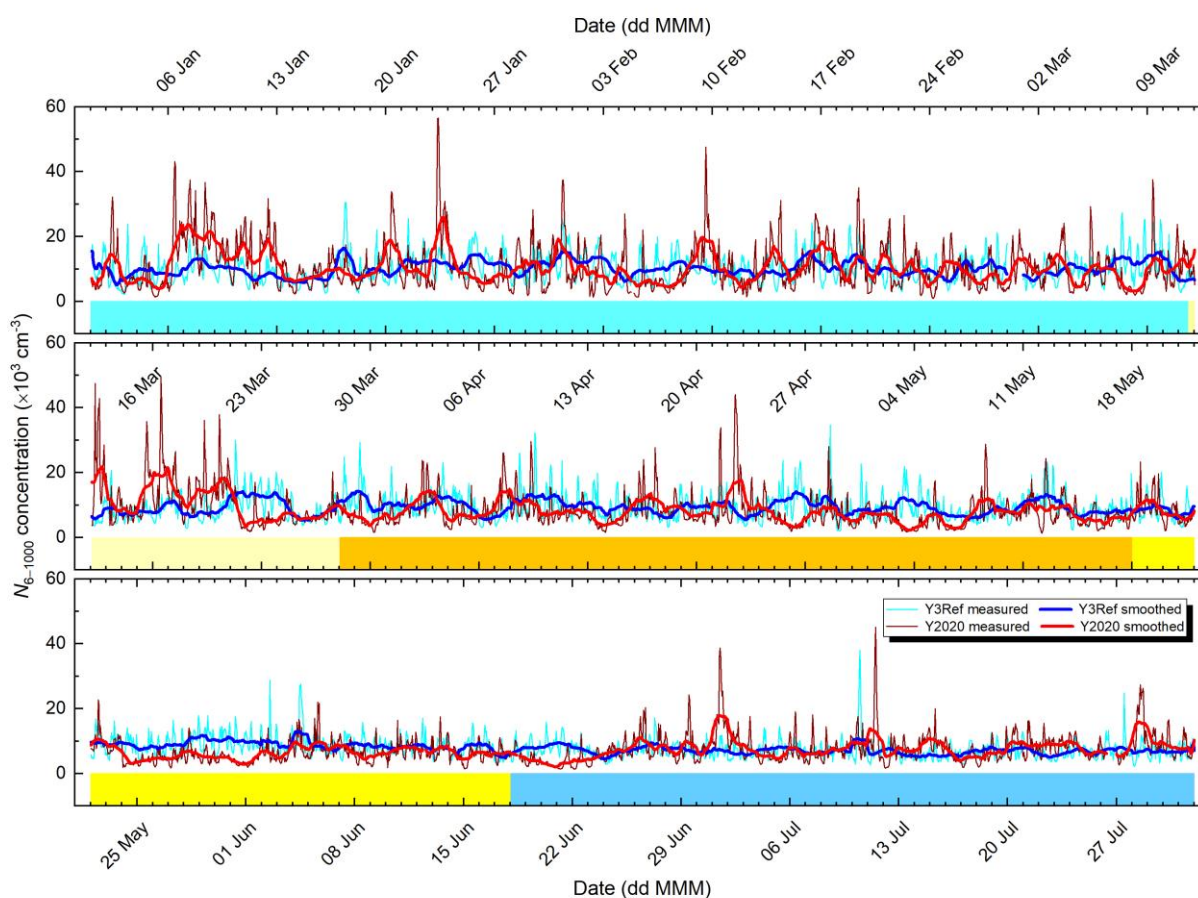
482



483 **Figure 5.** Time series of PM_{2.5} mass concentration in the average reference year of 2017–2019 (Y3Ref)
 484 and year 2020 together with their 24-h smoothed curves over the five consecutive phases of the first
 485 COVID-19 outbreak. The phases are marked by the following colour codes: Pre-emergency phase
 486 lighter blue, Pre-restriction phase lighter yellow, Restriction phase orange, Post-restriction phase darker
 487 yellow and Post-emergency phase darker blue. The tick labels of the abscissa indicate the Mondays in
 488 2020.

489

490 Many chemical species investigated originate from rather different sources. Nevertheless, their
 491 atmospheric concentrations often changed coherently, particularly in winter and early spring.
 492 A nice example is the interval of approximately 14–28 March 2020 when most species varied
 493 consistently. The MCPs for these days indicate strong anticyclonic weather types over the
 494 Carpathian Basin, stagnant and relatively calm meteorological conditions without precipitation
 495 in the area (Fig. S1). It is a confirmation of the common effects of regional meteorology on
 496 atmospheric concentrations, and that the daily evolution of meteorology can have higher
 497 influence on atmospheric concentrations than the source intensities under such specific
 498 conditions (Salma et al., 2020a). **Its consequences on the air quality are discussed in Sect. 3.8.**



518 **Figure 6.** Time series of N_{6-1000} concentration in the average reference year of 2017–2019 (Y3Ref) and
 519 year 2020 together with their 24-h smoothed curves over the five consecutive phases of the first
 520 COVID-19 outbreak. The phases are marked by the following colour codes: Pre-emergency phase
 521 lighter blue, Pre-restriction phase lighter yellow, Restriction phase orange, Post-restriction phase darker
 522 yellow and Post-emergency phase darker blue. The tick labels of the abscissa indicate the Mondays in
 523 2020.

524

525 The curves for PM_{2.5} mass and N_{6-1000} approved that there is weak association between these
526 two types of aerosol metrics (de Jesus et al., 2019). They are connected mainly via
527 meteorological properties, which is anyway active for all pollutants. It was sensible, therefore,
528 that both types of aerosol concentrations were included into the study as separate variables.

529 **3.4 Diurnal variations**

530 Average diurnal variations of NO, O₃, SO₂, PM_{2.5} mass and N_{6-100} **together with the vehicle**
531 **circulation** separately for workdays and holidays over the Restriction pandemic phase, for
532 which the differences in the shapes are expected to be the largest, are shown in Fig. 7 as
533 examples.

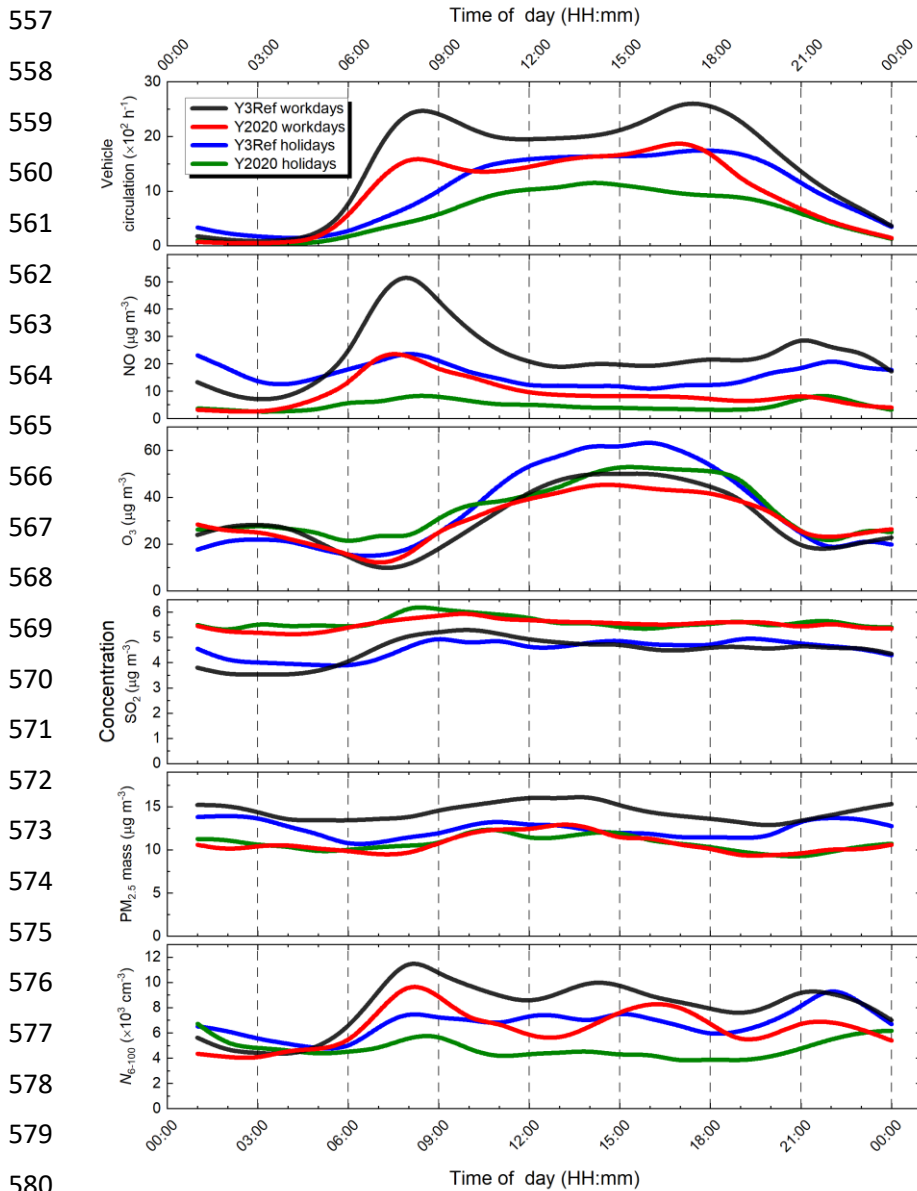
534

535 The curves of NO and N_{6-100} (together with NO₂, CO and N_{6-1000} , which are not shown)
536 followed the typical pattern of road traffic. They can largely be associated with vehicular
537 sources (tailpipe emissions, primary and secondary particles), and can advantageously be
538 applied for assigning potential concentration changes to traffic reduction. **It is seen that their**
539 **morning peak coincided with the peak of the morning rush hour, while their evening peak**
540 **appeared later than the peak of the afternoon rush hour. This shift could likely be related to the**
541 **daily evolution and cycling of the PBLH and to mixing intensity.** The curves of N_{6-100} contained
542 in addition the characteristic midday peak, which is caused by atmospheric NPF events. It is
543 worth realising that its position was shifted to later time. There were only nine quantifiable
544 NPF events during the Restriction phase in year 2020, which might not result in a representative
545 shape. An alternative explanation could be that this peak was caused by the overlapping effects
546 of direct traffic emissions and NPF events superimposed on each other. This experimental
547 observation should definitely be investigated and clarified when the necessary data sets become
548 available.

549

550 The curves for O₃ seemed to be opposite to NO as far as both their daily variations and the
551 orders of concentration magnitudes on workdays and holidays are concerned. These are in line
552 with the understanding of their atmospheric processes and coupled reaction mechanisms
553 (Jacob, 1999). In addition, the shapes in Y2020 seemed to be flattened with respect to Y3Ref.
554 The O₃ curves were also affected by the clock change, since the concentration of O₃ are
555 substantially influenced by solar radiation.

556



581 **Figure 7.** Average diurnal variations of motor vehicle road traffic in both directions on a major route
 582 (Váci Road) in Budapest and of NO, O₃, SO₂, PM_{2.5} mass and N₆₋₁₀₀ concentrations separately for
 583 workdays and holidays in the average reference year of 2017–2019 (Y3Ref) and year 2020 during the
 584 Restriction phase of the first COVID-19 outbreak.

585
 586 The curves for SO₂ (together with PM₁₀ mass and N₁₀₀₋₁₀₀₀, which are not shown) tracked the
 587 traffic pattern very loosely if at all. They could partially be related to traffic through diesel fuel,
 588 resuspension of urban dust by moving vehicles, dispersion of road surfaces, (non-exhaust)
 589 emissions from material wear of moving parts of vehicles and growth/ageing of particles
 590 emitted from vehicles (Salma and Maenhaut, 2006). Additional changes in the shape of the
 591 time variation of SO₂ could be caused by altered heating of and cooking at homes due to
 592 spreading practice of the work-from-home.

593

594 There was no obvious connection between the traffic and PM_{2.5} mass, which confirms our
595 earlier conclusion that the fine particles in Budapest mainly originate from non-vehicular
596 sources (Salma et al., 2020a).

597 **3.5 Quantification of concentration changes**

598 There are several mathematical statistical tests to determine whether atmospheric
599 concentrations over some time intervals in different years belong to the same distribution or
600 not. These methods, however, quantify the joint influence of all environmental effects (Sect.
601 1) and do not provide information on their causal relationships. The method described and
602 applied below allows to unfold some potential confounding influence of environmental
603 variables (e.g. PBLH) from concentration changes in order to gain a closer insight into the
604 source intensities of motor vehicles.

605

606 Median concentrations of pollutant gases and aerosol particles, median traffic circulation data
607 together with their relative differences and standardised anomaly values for the five pandemic
608 phases in the average reference year and year 2020 are summarised in Tables 2–6. It should be
609 noted that the standardised anomalies are rather small when recalling, for instance, the rigorous
610 concept of the limits of detection ($3\times SD$) and determination ($10\times SD$) in analytical chemistry.
611 This is largely caused by the strong dynamic features of related atmospheric properties and
612 processes (Sects. 1. and 3.3).

613

614 We showed in Sect. 3.1 that it is the PBLH_{max} of the meteorological conditions that likely
615 caused the largest side effects on the concentrations, and, therefore, its influence was taken into
616 account. A change in median concentrations for a pandemic phase was quantified to be
617 significant if both its relative difference fell outside the band of $[\pm 10 - f_{\text{mix}} \times \text{RDiff}(\text{PBLH}_{\text{max}})] \%$
618 and its SA_{ly} was outside the range of ± 0.3 . The multiplication factor f_{mix} accounts for non-
619 homogeneous mixing of pollutants within the boundary layer and for the effects of the daily
620 PBLH evolution. It was roughly estimated to be approximately 0.5. Its negative sign expresses
621 that atmospheric concentrations vary in a reciprocal manner with PBLH. The selected criteria
622 were based upon exercises with the data in the individual years 2017, 2018 and 2019. The
623 procedure represents a sensible and consequent approach, though alternative limits could also
624 be set.

625 **Table 2.** Median atmospheric concentrations of NO, NO₂ (both in units of $\mu\text{g m}^{-3}$) CO (mg m^{-3}), O₃,
626 SO₂, PM₁₀ mass, PM_{2.5} mass (all in $\mu\text{g m}^{-3}$), N_{6-1000} , N_{6-100} , N_{25-100} , $N_{100-1000}$ (all in 10^3 cm^{-3}) and median
627 vehicle road traffic (h^{-1}) on Szabadság Bridge, Váci Road, Széna Square and Alkotás Road in the
628 average reference year of 2017–2019 (Y3Ref) and year 2020 together with their relative difference
629 (RDiff, %) and their anomaly standardised to SD (SAly) for Pre-emergency phase of the first COVID-
630 19 outbreak. Chemical species with significant change are shown in bold.

631

Variable	Y3Ref	Y2020	RDiff	SAly
NO	31	18	-43	-0.5
NO ₂	51	40	-22	-0.7
CO	0.74	0.58	-21	-0.8
O₃	9.4	16	+68	+0.3
SO ₂	5.5	5.4	-1	-0.0
PM₁₀	45	29	-36	-1.2
PM_{2.5}	21	12	-42	-1.2
N_{6-1000}	9.5	8.8	-7	-0.2
N_{6-100}	7.2	6.8	-6	-0.1
N_{25-100}	3.5	3.1	-10	-0.2
$N_{100-1000}$	2.2	1.7	-21	-0.5
Szabadság B.	676	640	-5	-0.1
Váci R.	1589	1299	-18	-0.4
Széna S.	1374	1437	+5	+0.1
Alkotás R.	2517	2425	-4	-0.1

632

633 The Pre-emergency phase (Table 2) fitted completely into the heating season. The traffic flows
634 in city centre were identical, except for Váci Road, where it was somewhat lower in Y2020
635 than in Y3Ref. This could be caused by some local traffic arrangements. The PBLH_{max} increased
636 by 32 % (Table 1), which is substantial and affected the concentrations. Most concentration
637 changes were not significant. The exceptions were NO, O₃, PM₁₀ mass and PM_{2.5} mass, and
638 the latter two exhibited the largest anomalies. These two species have multiple sources. Organic
639 matter and elemental carbon, for instance, make up approximately 35 % of the PM_{2.5} mass in
640 winter (Salma et al., 2020a), and biomass burning is the major source of carbonaceous aerosol
641 in this season with an approximate relative contribution to the total carbon of 67 %. The share
642 of fossil-fuel combustion is around 25 %. This all implies that PM_{2.5} mass concentrations can
643 fluctuate extensively and irregularly in the heating season due to the source intensities. **The**
644 **reductions could also be related with changes in further meteorological properties such as T**

645 (mild February 2020, Fig. S4) or larger WS that acted on a shorter time scale than the pandemic
 646 phase (Fig. S3).

647

648 The higher O₃ concentration could partly be associated with the lower concentrations of NO.
 649 Ozone exhibits a strong seasonal dependency (Salma et al., 2020b). Lower concentrations in
 650 winter and early spring can be easily disturbed by its non-linear chemistry and by high WS.
 651 The modest SAly for O₃ suggests that this considerable relative concentration increase was
 652 mostly a consequence of low levels of O₃ in winter. The case nicely demonstrates the strength
 653 of and requirement for the coupled utilisation of RDiff and SAly criteria. Furthermore, the main
 654 differences in the concentrations appeared sporadically in an isolated manner. In addition, there
 655 was no coherence among the traffic-related variables. Therefore, all significant variations were
 656 interested as results of inter-annual variability in local meteorology, emissions and formation
 657 processes.

658

659 **Table 3.** Median atmospheric concentrations of NO, NO₂ (both in units of µg m⁻³) CO (mg m⁻³), O₃,
 660 SO₂, PM₁₀ mass, PM_{2.5} mass (all in µg m⁻³), N₆₋₁₀₀₀, N₆₋₁₀₀, N₂₅₋₁₀₀, N₁₀₀₋₁₀₀₀ (all in 10³ cm⁻³) and median
 661 vehicle road traffic (h⁻¹) on Szabadság Bridge, Váci Road, Széna Square and Alkotás Road in the
 662 average reference year of 2017–2019 (Y3Ref) and year 2020 together with their relative difference
 663 (RDiff) in % and their anomaly standardised to SD (SAly) for Pre-restriction phase of the first COVID-
 664 19 outbreak. Chemical species with significant change are shown in bold.

665

Variable	Y3Ref	Y2020	RDiff	SAly
NO	20	12	-39	-0.3
NO₂	46	38	-18	-0.5
CO	0.60	0.56	-8	-0.2
O₃	18	33	+80	+0.7
SO ₂	5.1	5.4	+7	+0.3
PM ₁₀	34	30	-12	-0.3
PM_{2.5}	19	13	-32	-0.8
N ₆₋₁₀₀₀	8.1	8.4	+4	+0.1
N ₆₋₁₀₀	6.7	6.9	+4	+0.1
N ₂₅₋₁₀₀	2.9	3.2	+9	+0.1
N ₁₀₀₋₁₀₀₀	1.4	1.6	+11	+0.2
Szabadság B.	652	417	-36	-0.8
Váci R.	1522	939	-38	-0.7
Széna S.	1371	1001	-27	-0.5
Alkotás R.	2792	1925	-31	-0.7

666 The Pre-restriction phase (Table 3) was rather short (16 days), and, therefore, its interpretation
 667 should be approached with a special caution due to some issues in representativity. It was also
 668 completely part of the heating season, and the extreme drought in the Carpathian Basin in 2020
 669 could also play a role. The PBLH_{max} was almost identical in both years (Table 1). The
 670 concentrations of NO₂, PM_{2.5} mass and perhaps NO declined, while O₃ was enhanced.
 671 Excitingly, CO did not show substantial decrease. The changes could be affected by lower
 672 traffic during its last half/week (Fig. 2) and increased GRad.

673

674 **Table 4.** Median atmospheric concentrations of NO, NO₂ (both in units of $\mu\text{g m}^{-3}$) CO (mg m^{-3}), O₃,
 675 SO₂, PM₁₀ mass, PM_{2.5} mass (all in $\mu\text{g m}^{-3}$), N_{6-1000} , N_{6-100} , N_{25-100} , $N_{100-1000}$ (all in 10^3 cm^{-3}) and median
 676 vehicle road traffic (h^{-1}) on Szabadság Bridge, Váci Road, Széna Square and Alkotás Road in the
 677 average reference year of 2017–2019 (Y3Ref) and year 2020 together with their relative difference
 678 (RDiff) in % and their anomaly standardised to SD (SAly) for Restriction phase of the first COVID-19
 679 outbreak. Chemical species with significant change are shown in bold.

680

Variable	Y3Ref	Y2020	RDiff	SAly
NO	19	6.0	-68	-0.5
NO₂	44	26	-39	-1.1
CO	0.58	0.43	-27	-0.8
O ₃	31	35	+13	+0.2
SO ₂	5.4	5.5	+3	+0.1
PM ₁₀	32	28	-13	-0.3
PM_{2.5}	14	11	-22	-0.4
N_{6-1000}	8.8	6.7	-24	-0.5
N_{6-100}	7.4	5.3	-28	-0.6
N_{25-100}	3.2	2.8	-12	-0.2
$N_{100-1000}$	1.3	1.2	-5	+0.1
Szabadság B.	689	318	-54	-1.2
Váci R.	1626	803	-51	-1.0
Széna S.	1537	844	-45	-1.0
Alkotás R.	3031	1516	-50	-1.1

681

682 The beginning one-third part of the Restriction phase (Table 4) fell into the heating season, and
 683 it was fully incorporated into the extremely dry weather season. The vehicle flows were
 684 reduced by approximately half uniformly at all urban locations. Concentrations of NO, NO₂,
 685 CO, PM_{2.5} mass, N_{6-1000} and N_{6-100} changed significantly, and they all declined. The alterations
 686 happened in a systematic or continuous manner in time (Figs. 2–6, S6 and S7). These species

687 can be associated with vehicular road traffic. Except for PM_{2.5} mass, which is linked more to
688 household and residential sources. At the same time, some other important pollutants such as
689 $N_{100-1000}$ or SO₂ – which are typically related to larger spatial extent or region and which could,
690 therefore, be influenced by meteorology – did not change significantly. Similar reductions were
691 reported for other urban locations in the world (Keller et al., 2020; Lal et al., 2020; Le et al.,
692 2020; Lee et al., 2020; Tobías et al., 2020). This all can be interpreted that the alterations in
693 NO, NO₂, CO, N_{6-1000} and N_{6-100} concentrations were primarily caused by the lower vehicular
694 traffic intensity in the city, and that the PBLH could also contribute by approximately 9 % in
695 an absolute sense (Table 1). The increased O₃ can be explained by its production from volatile
696 organic compounds (VOCs) and NO_x in the VOC-limited chemical regime even under
697 decreasing NO_x conditions (Jacob, 1999; Lelieveld and Dentener, 2000): This regime is typical
698 for many large cities. The VOCs can involve, for instance, aromatics such as benzene and
699 toluene, which largely originate from traffic sources.

700

701 **Table 5.** Median atmospheric concentrations of NO, NO₂ (both in units of $\mu\text{g m}^{-3}$) CO (mg m^{-3}), O₃,
702 SO₂, PM₁₀ mass, PM_{2.5} mass (all in $\mu\text{g m}^{-3}$), N_{6-1000} , N_{6-100} , N_{25-100} , $N_{100-1000}$ (all in 10^3 cm^{-3}) and median
703 vehicle road traffic (h^{-1}) on Szabadság Bridge, Váci Road, Széna Square and Alkotás Road in the
704 average reference year of 2017–2019 (Y3Ref) and year 2020 together with their relative difference
705 (RDiff) in % and their anomaly standardised to SD (SAly) for Post-restriction phase of the first COVID-
706 19 outbreak. Chemical species with significant change are shown in bold.

707

Variable	Y3Ref	Y2020	RDiff	SAly
NO	12	6.4	-44	-0.2
NO₂	40	26	-35	-0.9
CO	0.48	0.42	-13	-0.3
O ₃	42	37	+11	-0.2
SO₂	4.7	5.9	+26	+1.0
PM₁₀	29	21	-28	-0.6
PM_{2.5}	12	9.3	-24	-0.4
N_{6-1000}	8.2	6.0	-27	-0.5
N_{6-100}	6.8	4.9	-27	-0.5
N_{25-100}	3.3	2.4	-27	-0.5
$N_{100-1000}$	1.3	1.0	-22	-0.3
Szabadság B.	670	575	-14	-0.3
Váci R.	1536	1137	-26	-0.5
Széna S.	1540	1387	-10	-0.2
Alkotás R.	2597	2281	-12	-0.2

708

709 In the Post-restriction phase (Table 5), the vehicle flow recovered step wisely. The $PBLH_{max}$
710 in Y2020 decreased substantially relative to Y3Ref (Table 1). Most chemical species such as
711 NO_2 , SO_2 , PM_{10} mass, $PM_{2.5}$ mass, N_{6-1000} , N_{6-100} , N_{25-100} and $N_{100-1000}$ exhibited significant
712 changes. The list also included variables which characterize the region. At the same time, some
713 typical vehicular-related species such as NO and CO – which are not really water soluble –
714 were not among them. Most significant changes showed decreasing tendency, except for SO_2
715 which increased. The latter was caused by a continuously increasing SO_2 concentration (Fig.
716 S8), recorded at the other air quality monitoring stations as well. The increase was likely caused
717 as a perturbation by some local sources in the upwind direction from the city. This all suggests
718 that the alterations were mainly produced by arrival of continued and spatially extended rains
719 in its second half of the pandemic phase (Fig. S1). The precipitation washed out many chemical
720 species from the urban and regional atmospheres. This time interval unambiguously
721 demonstrated that the regional weather can cause similar modifications in atmospheric
722 concentrations as a substantially reduced (by 50 %) urban traffic.

723

724 In the Post-emergency phase (Table 6), the traffic was at its ordinary level and there were no
725 larger weather alternations. Most concentrations – including some major vehicle-related
726 pollutants such as CO and N_{6-100} – did not change significantly. The exceptions were NO , NO_2 ,
727 O_3 and $PM_{2.5}$ mass. The first three variables are connected to each other through atmospheric
728 chemistry. The changes can likely be linked to inter-annual variability in sources, sinks,
729 meteorological properties that act on a shorter time scale than the pandemic phase and
730 atmospheric transformation and transport – similarly to that observed in the Pre-emergency
731 phase.

732

733 **Table 6.** Median atmospheric concentrations of NO, NO₂ (both in units of µg m⁻³) CO (mg m⁻³), O₃,
734 SO₂, PM₁₀ mass, PM_{2.5} mass (all in µg m⁻³), *N*₆₋₁₀₀₀, *N*₆₋₁₀₀, *N*₂₅₋₁₀₀, *N*₁₀₀₋₁₀₀₀ (all in 10³ cm⁻³) and median
735 vehicle road traffic (h⁻¹) on Szabadság Bridge, Váci Road, Széna Square and Alkotás Road in the
736 average reference year of 2017–2019 (Y3Ref) and year 2020 together with their relative difference
737 (RDiff) in % and their anomaly standardised to SD (SAly) for Post-emergency phase of the first
738 COVID-19 outbreak. Chemical species with significant change are shown in bold.
739

Variable	Y3Ref	Y2020	RDiff	SAly
NO	16	7.4	-54	-0.3
NO₂	39	27	-31	-0.7
CO	0.43	0.42	-2	-0.1
O₃	39	46	+17	+0.3
SO ₂	4.0	4.3	+9	+0.3
PM ₁₀	26	22	-15	-0.3
PM_{2.5}	12	9.1	-22	-0.3
<i>N</i> ₆₋₁₀₀₀	6.7	6.7	+0	+0.0
<i>N</i> ₆₋₁₀₀	5.5	5.4	-2	-0.0
<i>N</i> ₂₅₋₁₀₀	2.7	2.8	+5	+0.1
<i>N</i> ₁₀₀₋₁₀₀₀	1.1	1.2	+9	+0.1
Szabadság B.	690	663	-4	-0.1
Váci R.	1471	1218	-17	-0.3
Széna S.	1594	1511	-5	-0.1
Alkotás R.	2507	2531	+1	+0.0

740 3.6 Change rates

741 Linear regression analysis between the median RDiff for vehicle traffic on one side and RDiff
742 for pollutants corrected for the RDiff(PBLH_{max}) on the other side for all pandemic phases
743 yielded change rates and SDs for NO, NO₂, *N*₆₋₁₀₀₀ and CO were 0.63±0.23, 0.57±0.14,
744 0.40±0.17 and 0.22±0.08, respectively. For PM₁₀ mass and PM_{2.5} mass, the rates were slightly
745 negative and insignificant. The data points for the Post-restriction phase – which were
746 substantially affected by precipitation and frontal weather systems – were excluded from this
747 analysis.

748

749 The change rates suggest that nitrogen-oxides vary sensitively with traffic, total particle
750 number concentration shows considerable dependency, while variation of CO is modest. This
751 is linked to their residence times as well. The PM mass concentrations do not appear to be
752 closely related to traffic intensity in central Budapest.

753 3.7 Spatial gradients

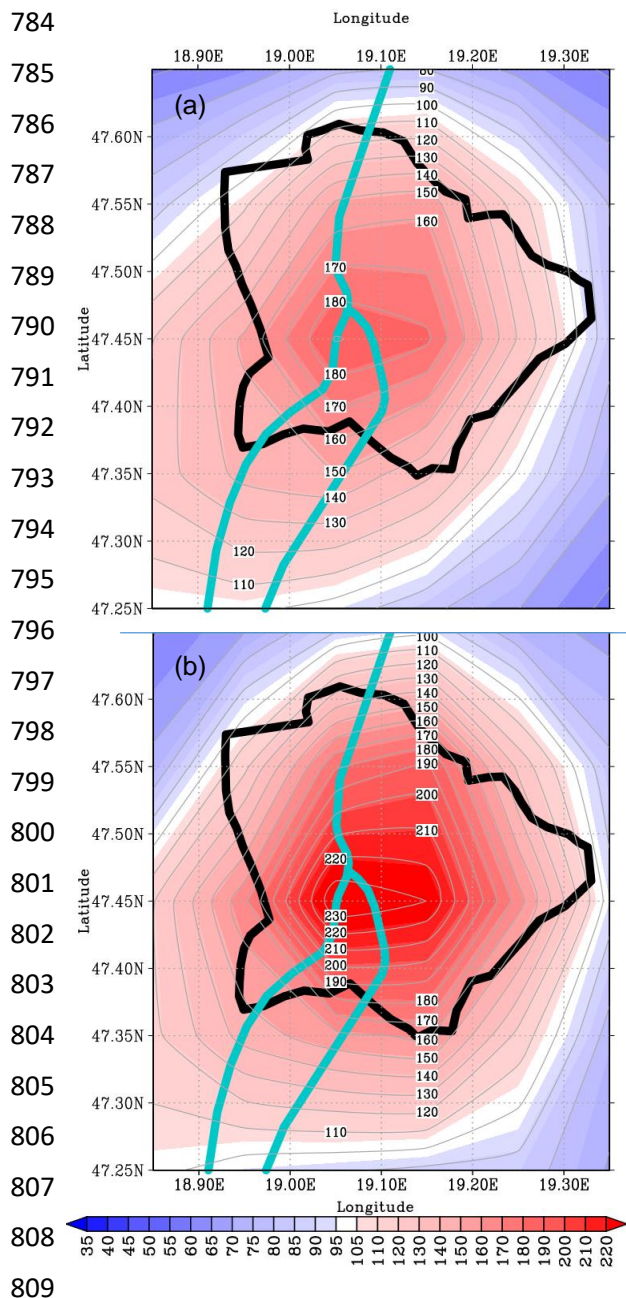
754 Spatial distributions of NO and O₃ derived by CAMS ensemble reanalysis in 2018–2019 and
755 2020 during the Restriction pandemic phase are shown in Figs. 8 and 9 as examples. The
756 absolute concentrations can be different from the measured values due to the specialities in the
757 applied models, while the relative tendencies are expected to be expressed correctly. Figure 8
758 indicates that the differences from the corresponding median (spatial gradients) in 2020 were
759 larger than in 2018–2019. This can be explained if the relative concentration changes at the
760 outer parts of the city or near-city background were even larger than in the centre. The spatial
761 distribution of NO₂ was similar to NO, although its gradients were smaller than for NO. Spatial
762 distributions of CO and PM_{2.5} mass were featureless and similar to each other in 2018–2019
763 and 2020.

764
765 Spatial distributions of O₃ (Fig. 9) and, perhaps SO₂ (which is not shown), exhibited relative
766 decrease in the centre, which gradients were relatively small and similar to each other for both
767 time intervals. This all is in line with the tendencies observed in their measured concentrations
768 (Sects. 3.3 and 3.4). We are aware that several pollutants originate from diffusive line sources,
769 which can be enriched along roads and, therefore, much larger concentration gradients can
770 occur on smaller spatial scales.

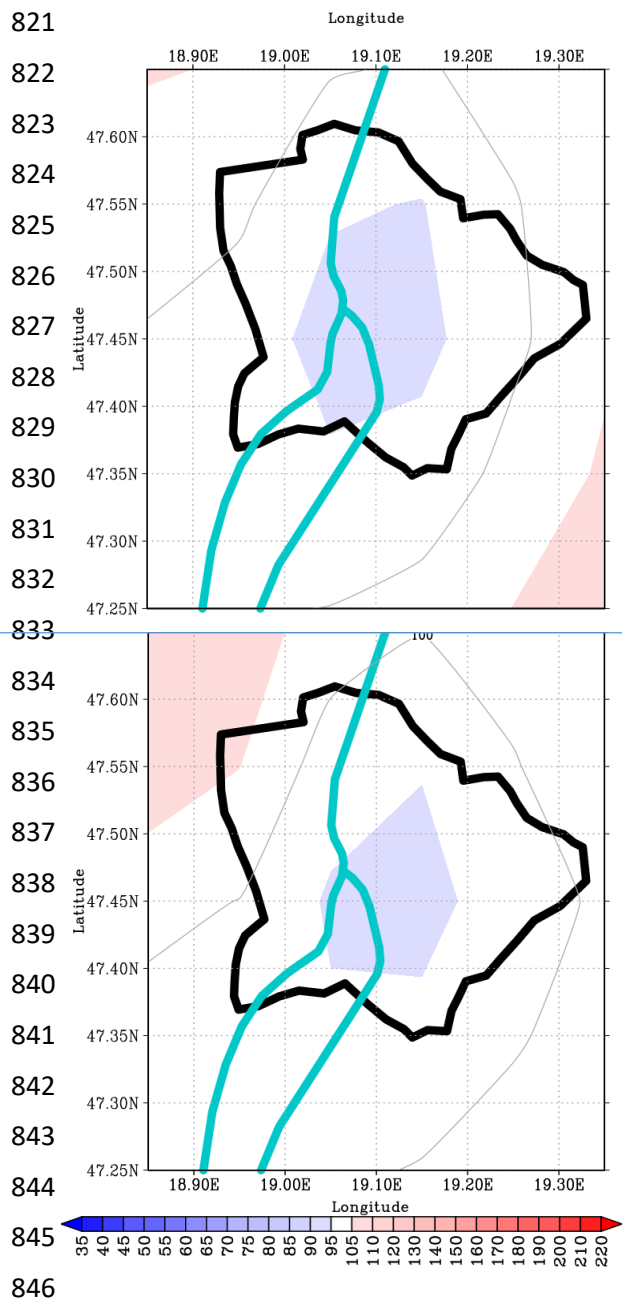
771 3.8 Potentials for improving air quality

772 In order to assess the importance of concentration changes that could be achieved by
773 tranquilizing the vehicle road traffic in Budapest, the atmospheric concentrations and their
774 possible decrements were compared to various limit values (EU Directives, 2008; VM 4, 2011).

775
776 NO₂ exhibited the most frequent exceedances of standards for the protection of health. Its
777 concentrations in 2017, 2018 and 2019 were larger in 172, 155 and 61 cases than the 1-h
778 national health limit of 100 µg m⁻³ (Fig. S6). The permitted number of exceedances is 18 a
779 year. It is mentioned that this concentration limit is 200 µg m⁻³ for the EU, which would be
780 fulfilled completely. The NO₂ excess usually remained modest – particularly when contrasted
781 to the smog alert thresholds of 350 (for the warning state) and 400 µg m⁻³ (for the alarm state).
782 The daily health limit of 85 µg m⁻³ was also exceeded in 6, 2 and 0 days in the three years,
783 respectively. A reduction of 6 % in NO₂ concentration (that corresponds to a 10 %-decline in



810 **Figure 8.** Spatial distribution of median NO
 811 concentration in Budapest in 2018–2019 (a)
 812 and 2020 (b) during the Restriction phase of
 813 the first COVID-19 outbreak obtained from
 814 CAMS ensemble reanalysis. The
 815 concentrations were normalised to the overall
 816 spatial median concentrations of 0.93 and
 817 $0.59 \mu\text{g m}^{-3}$, respectively. The border of the
 818 city and the Danube River are indicated with
 819 curves in black and blue colour, respectively
 820 for better orientation.



847 **Figure 9.** Spatial distribution of median O₃
 848 concentration in Budapest in 2018–2019 (a)
 849 and 2020 (b) during the Restriction phase of
 850 the first COVID-19 outbreak obtained from
 851 CAMS ensemble reanalysis. The
 852 concentrations were normalised to the overall
 853 spatial median concentrations of 60 and $67 \mu\text{g}$
 854 m^{-3} , respectively. The border of the city and
 855 the Danube River are indicated with curves in
 856 black and blue colour, respectively for better
 857 orientation.

858 in vehicle circulation) would decrease the number of exceedances of the 1-h national health
859 limit typically to 114, 98 and 42, respectively, while the number of days above the daily health
860 limit would be lowered to 2, 0 and 0, respectively.

861

862 Less frequent though more severe exceedances than for NO₂ happened for PM₁₀ mass (Fig.
863 S9). The daily mean PM₁₀ mass concentrations in 2017, 2018 and 2019 exceeded the daily
864 health limit of 50 µg m⁻³ in 36, 93 and 57 days, respectively at this actual air quality monitoring
865 station. Most exceedances occurred in the heating season. Their permitted number is 35 a year.
866 The smog alert thresholds for the warning and alarm states are 75 and 100 µg m⁻³, respectively.
867 The number of exceedances for the warning stage were 12, 17 and 9, respectively. It should be
868 added that smog alerts are announced on the basis of a complex set of conditions which include
869 larger numbers of monitoring stations and days. As a matter of fact, the warning state was
870 announced 3 times for 11 days in total and once for 2 days in 2017 and 2018, respectively.
871 There was no smog alert in 2019. It is stressed that all alarm states since 2007 were announced
872 exclusively because of high PM₁₀ mass concentrations, and all alert intervals were confined to
873 winter. This points to the role of local and regional meteorology and other sources than vehicle
874 traffic (Salma et al., 2020a). There is cold air pool that develops from time to time above the
875 Carpathian Basin in winter, which generates a lasting *T* inversion and a shallow planetary
876 boundary layer, restricts the vertical mixing and results in poor air quality over extended areas
877 of the basin in larger and smaller cities as well as in rural areas.

878

879 All O₃ concentrations were below the maximum daily 8-h health limit of 120 µg m⁻³ (Fig. 4).
880 The concentrations of CO were far away from both the 1-h and maximum daily 8-h health
881 limits of 10 and 5 mg m⁻³, respectively (Fig. S7), and the situation was similar for SO₂, for
882 which the 1-h and daily limits are 250 and 125 µg m⁻³, respectively (Fig. S8).

883 **4 Conclusions**

884 The relationships between urban air quality and motor vehicle road traffic are not
885 straightforward since the contributions of traffic flow to pollutants concentrations are
886 superimposed in the variability in local meteorological conditions, long-range transport of air
887 masses and other sources/sinks. We introduced here an approach based on both relative
888 difference and standardised anomaly, which helps unfolding some important confounding
889 environmental factors. It can support creating a generalised picture on urban atmospheres.

890

891 The method was deployed on the Budapest data during the different phases of the first COVID-
892 19 outbreak. Various restriction measures introduced due to the pandemic resulted in a decline
893 of vehicle road traffic down to approximately 50 % during the severest limitations. In parallel,
894 concentrations of NO, NO₂, CO, N_{6-1000} and N_{6-100} decreased substantially, some other species
895 such as PM_{2.5} mass, PM₁₀ mass and $N_{100-1000}$ changed modestly and inconclusively, while O₃
896 showed an increasing tendency. Change rates of NO and NO₂ with relative change of traffic
897 intensity (~~formally expressed as %/%~~) were the largest (approximately 0.6), total particle
898 number concentration showed considerable dependency (0.4), while variation of CO was
899 modest (0.2). It was demonstrated that a similar decrease in concentrations as observed in the
900 strictest pandemic phase can also be caused by other (natural/meteorological) effects than
901 traffic. The rainy weather in June 2020 (the so-called St. Medard's forty days of rain in Central
902 European folklore) yielded, for instance, very similar low pollution levels.

903

904 The study revealed that intentional reduction of traffic intensity can have unambiguous
905 potentials in improving urban air quality as far as NO, NO₂, CO and particle number
906 concentrations are concerned. It should be added that ~~all smog alerts in Budapest were~~
907 ~~exclusively announced because of the most critical pollutant in many European cities including~~
908 ~~Budapest, namely the PM₁₀ mass, however, which~~ did not seem to be considerably affected
909 by vehicle flow. Nevertheless, measures for tranquillizing urban traffic can contribute to
910 improved air quality through a new strategy for lowering the population exposure of inhabitants
911 instead of high-risk management of individuals.

912

913 The method could be expanded by other important ordinary chemical species such as soot and
914 by other location types such as near-city or regional background sites jointly with central
915 locations in order to obtain more exact meteorology-normalized changes. The results also point
916 to the importance of non-linear relationships among precursors and secondary pollutants,
917 which are to be further studied to gain better insights into urban atmospheric chemistry and air
918 quality issues. ~~Finally, it should be mentioned that contemporary urban air quality and climate~~
919 ~~issues and their related policies are largely biased by financing possibilities and economic~~
920 ~~performance/growth.~~

921

922 *Data availability.* The observational data are accessible at <http://www.levegominoseg.hu/> or are
923 available from the corresponding author – except for the vehicle road traffic – upon request.

924
925
926
927
928
929
930
931
932
933
934
935
936
937
938
939
940
941
942

943

944
945
946
947
948
949
950
951
952
953
954
955
956
957
958
959
960
961
962
963
964
965
966
967
968
969

Supplement. The supplement related to this article is available online.

Author contributions. IS conceived the study. AZGy, WT and IS performed most aerosol and meteorological measurements. All co-authors participated in the data processing and interpreting the results. The figures were created by MV and AZGy. IS wrote the manuscript with comments from all coauthors.

Competing interests. The authors declare that they have no conflict of interest.

Acknowledgements. The authors thank the leaders of the Budapest Public Roads Ltd. (Budapest Közút Zrt.) for providing the vehicle road traffic data and its coworker Dezső Huszár for valuable discussions. The map in Fig. 1 was created by Márton Pál, Ph. D. student of the Department of Cartography and Geoinformatics, Eötvös University. The authors are grateful to Attila Machon (Hungarian Meteorological Service) for his help with the criteria air pollutant data.

Financial support. This research was supported by the Hungarian Research, Development and Innovation Office (grant nos. K116788 and K132254) and by the European Regional Development Fund and the Hungarian Government (GINOP-2.3.2-15-2016-00055).

References

- C3S (Copernicus Climate Change Service), ERA5: Fifth generation of ECMWF atmospheric reanalyses of the global climate, Copernicus Climate Change Service Climate Data Store, 2017, URL: cds.climate.copernicus.eu, last access 1 August 2020.
- CAMS (Copernicus Atmosphere Monitoring Service), User Guide: Regional Air Quality Data Server, Fundamentals on production and services, Report issued by Météo-France, 2019, https://www.regional.atmosphere.copernicus.eu/doc/USER_GUIDE_dataServer.pdf, last accessed 27 August 2020.
- de Jesus, A. L., Rahman, M. M., Mazaheri, M., Thompson, H., Knibbs, L. D., Jeong, C., Evans, G., Nei, W., Ding, A., Qiao, L., Li, L., Portin, H., Niemi, J. V., Timonen, H., Luoma, K., Petäjä, T., Kulmala, M., Kowalski, M., Peters, A., Cyrys, J., Ferrero, L., Manigrasso, M., Avino, P., Buonano, G., Reche, C., Querol, X., Beddows, D., Harrison, R. M., Sowlat, M. H., Sioutas, C., and Morawska, L.: Ultrafine particles and PM_{2.5} in the air of cities around the world: Are they representative of each other?, *Environ. Int.*, 129, 118–135, 2019.
- Conticini, E., Frediani, B., and Caro, D.: Can atmospheric pollution be considered a co-factor in extremely high level of SARS-CoV-2 lethality in Northern Italy?, *Environ. Pollut.*, 261, 114465, 2020.
- EU Directives, Directive 2008/50/EC of the European Parliament and of the Council of 21 May 2008 on ambient air quality and cleaner air for Europe, *Off. J. EU*, L 152, 11.6.2008, pp. 1–44, 2008.
- Frontera, A., Cianfanelli, L., Vlachos, K., Landoni, G., and Cremona, G.: Severe air pollution links to higher mortality in COVID-19 patients: The “double-hit” hypothesis, *J. Infection*, in press, 2020.
- Gentner, D. R., Jathar, S. H., Gordon, T. D., Bahreini, R., Day, D. A., El Haddad, I., Hayes, P. L., Pieber, S. M., Platt, S. M., de Gouw, J., Goldstein, A. H., Harley, R. A., Jimenez, J. L., Prévôt, A. S. H., and Robinson, A. L.: Review of urban secondary organic aerosol formation from gasoline and diesel motor vehicle emissions, *Environ. Sci. Technol.*, 51, 1074–1093, 2017.
- Harrison, R. M.: Urban atmospheric chemistry: a very special case for study, *Clim. Atmos. Sci.*, 1, 20175, 2018, <https://doi.org/10.1038/s41612-017-0010-8>.

970 Harrison, R. M., Jones, A. M., Gietl, J., Yin, J. and Green, D. C.: Estimation of the contributions of
971 brake dust, tire wear, and resuspension to nonexhaust traffic particles derived from atmospheric
972 measurements, *Environ. Sci. Technol.*, 46, 6523–6529, 2012.

973 Hopke, Ph. K.: Review of receptor modeling methods for source apportionment, *J. Air Waste*
974 *Manage.*, 66, 237–259, 2016.

975 Horvath, H., Kreiner, I., Norek, C., Preining O., and Georgi, B.: Diesel emissions in Vienna, *Atmos.*
976 *Environ.*, 22, 1255–1269, 1988.

977 Jacob, J. J.: *Introduction to Atmospheric Chemistry*, Princeton University Press, Cambridge, 1999.

978 Keller, C. A., Evans, M. J., Knowland, K. E., Hasenkopf, C. A., Modekurty, S., Lucchesi, R. A., Oda,
979 T., Franca, B. B., Mandarino, F. C., Díaz Suárez, M. V., Ryan, R. G., Fakes, L. H., and Pawson,
980 S.: Global Impact of COVID-19 Restrictions on the Surface Concentrations of Nitrogen Dioxide
981 and Ozone, *Atmos. Chem. Phys. Discuss.*, <https://doi.org/10.5194/acp-2020-685>, in review, 2020.

982 Lal, P., Kumar, A., Kumar, S., Kumari, S., Saikia, P., Dayanandan, A., Adhikari, D., and Khane, M.
983 L.: The dark cloud with a silver lining: Assessing the impact of the SARS COVID-19 pandemic on
984 the global environment, *Sci. Total Environ.*, 732, 139297, 2020.

985 Le, T., Wang, Y., Liu, L., Yang, J., Yung, Y. L., Li, G., and Seinfeld, J. H.: Unexpected air pollution
986 with marked emission reductions during the COVID-19 outbreak in China, *Science*, 369, 702–706,
987 2020.

988 Lee, J. D., Drysdale, W. S., Finch, D. P., Wilde, S. E., and Palmer, P. I.: UK surface NO₂ levels
989 dropped by 42% during the COVID-19 lockdown: impact on surface O₃, *Atmos. Chem. Phys.*
990 *Discuss.*, <https://doi.org/10.5194/acp-2020-838>, in review, 2020.

991 Lelieveld, J. and Dentener, F. J.: What controls tropospheric ozone?, *J. Geophys. Res., Atmos.*, 105,
992 3531–3551, 2000.

993 Liu, Y., Ning, Z., Chen, Y., Guo, M., Liu, Y., Gali, N. K., Sun, L., Duan, Y., Cai, J., Westerdahl, D.,
994 Liu, X., Xu, K., Ho, K., Kan, H., Fu, Q., and Lan, K.: Aerodynamic analysis of SARS-CoV-2 in
995 two Wuhan hospitals, *Nature* 582, 557–560, 2020.

996 Mahato, S., Pal, S., and Ghosh, K. G.: Effect of lockdown amid COVID-19 pandemic on air quality of
997 the megacity Delhi, India, *Sci. Total Environ.*, 730, 39086, doi:10.1016/j.scitotenv.2020.139086,
998 2020.

999 Maheras, P., Tolika, K., Tegoulas, I., Anagnostopoulou, Ch., Szpirosz, K., Károssy, Cs., and Makra,
1000 L.: Comparison of an automated classification system with an empirical classification of
1001 circulation patterns over the Pannonian basin, Central Europe, *Meteorol. Atmos. Phys.*,
1002 <https://doi.org/10.1007/s00703-018-0601-x>, 2018.

1003 Marécal, V., Peuch, V.-H., Andersson, C., Andersson, S., Arteta, J., Beekmann, M., Benedictow, A.,
1004 Bergström, R., Bessagnet, B., Cansado, A., Chéroux, F., Colette, A., Coman, A., Curier, R. L.,
1005 Denier van der Gon, H. A. C., Drouin, A., Elbern, H., Emili, E., Engelen, R. J., Eskes, H. J., Foret,
1006 G., Friese, E., Gauss, M., Giannaros, C., Guth, J., Joly, M., Jaumouillé, E., Josse, B., Kadygrov,
1007 N., Kaiser, J. W., Krajsek, K., Kuenen, J., Kumar, U., Liora, N., Lopez, E., Malherbe, L.,
1008 Martinez, I., Melas, D., Meleux, F., Menut, L., Moinat, P., Morales, T., Parmentier, J., Piacentini,
1009 A., Plu, M., Poupkou, A., Queguiner, S., Robertson, L., Rouïl, L., Schaap, M., Segers, A., Sofiev,
1010 M., Thomas, M., Timmermans, R., Valdebenito, Á., van Velthoven, P., van Versendaal, R., Vira,
1011 J., and Ung, A.: A regional air quality forecasting system over Europe: The MACC-II daily
1012 ensemble production, *Geosci. Model Dev.*, 8, 2777–2813, 2015.

1013 Mikkonen, S., Németh, Z., Varga, V., Weidinger, T., Leinonen, V., Yli-Juuti, T., and Salma, I.:
1014 Decennial time trends and diurnal patterns of particle number concentrations in a central European
1015 city between 2008 and 2018, *Atmos. Chem. Phys.*, 20, 12247–12263, 2020.

1016 Morawska, L. and Cao, J.: Airborne transmission of SARS-CoV-2: The world should face the reality,
1017 *Environ. Int.*, 139, 105730, <https://doi.org/10.1016/j.envint.2020.105730>, 2020.

1018 Nakada, L. Y. K. and Urban, R. C.: COVID-19 pandemic: Impacts on the air quality during the partial
1019 lockdown in São Paulo state, Brazil, *Sci. Total Environ.*, 730, 139087, 2020.

1020 Paasonen, P., Kupiainen, K., Klimont, Z., Visschedijk, A., Denier van der Gon, H. A. C., and Amann,
1021 M.: Continental anthropogenic primary particle number emissions, *Atmos. Chem. Phys.*, 16, 6823–
1022 6840, 2016.

1023 Péczely, Gy.: Grosswetterlagen in Ungarn (Large-scale weather situations in Hungary, in German),
1024 Publication of the Hungarian Meteorological Institute, 30, pp. 86, Budapest, 1957.

1025 Petetin, H., Bowdalo, D., Soret, A., Guevara, M., Jorba, O., Serradell, K., and Pérez García-Pando, C.:
1026 Meteorology-normalized impact of COVID-19 lockdown upon NO₂ pollution in Spain, *Atmos.*
1027 *Chem. Phys. Discuss.*, 2020, 1–29, 10.5194/acp-2020-446, 2020.

1028 Putaud, J.-P., Van Dingenen, R., Alastuey, A., Bauer, H., Birmili, W., Cyrus, J., Flentje, H., Fuzzi, S.,
1029 Gehrig, R., Hansson, H. C., Harrison, R. M., Herrmann, H., Hitzenberger, R., Hüglin, C., Jones, A.
1030 M., Kasper-Giebl, A., Kiss, G., Koussa, A., Kuhlbusch, T. A. J., Löschau, G., Maenhaut, W.,
1031 Molnár, A., Moreno, T., Pekkanen, J., Perrino, C., Pitz, M., Puxbaum, H., Querol, X., Rodriguez,
1032 S., Salma, I., Schwarz, J., Smolík, J., Schneider, J., Spindler, G., ten Brink, H., Turšič, J., Viana,
1033 M., Wiedensohler, A., and Raes, F.: A European Aerosol Phenomenology - 3: physical and
1034 chemical characteristics of particulate matter from 60 rural, urban, and kerbside sites across
1035 Europe, *Atmos. Environ.*, 44, 1308–1320, 2010.

1036 Rönkkö, T., Kuuluvainen, H., Karjalainen, P., Keskinen, J., Hillamo, R., Niemi, J. V., Pirjola, L.,
1037 Timonen, H. J., Saarikoski, S., Saukko, E., Järvinen, A., Silvennoinen, H., Rostedt, A., Olin, M.,
1038 Yli-Ojanperä, J., Nousiainen, P., Koussa, A., and Dal Maso, M.: Traffic is a major source of
1039 atmospheric nanocluster aerosol, *Proc. Natl. Acad. Sci. USA*, 114, 7549–7554, 2017.

1040 Salma, I. and Maenhaut, W.: Changes in chemical composition and mass of atmospheric aerosol
1041 pollution between 1996 and 2002 in a Central European city, *Environ. Pollut.*, 143, 479–488,
1042 2006.

1043 Salma, I. and Németh, Z.: Dynamic and timing properties of new aerosol particle formation and
1044 consecutive growth events, *Atmos. Chem. Phys.*, 19, 5835–5852, 2019.

1045 Salma, I., Borsós, T., Németh, Z., Weidinger, T., Aalto, T., and Kulmala, M.: Comparative study of
1046 ultrafine atmospheric aerosol within a city, *Atmos. Environ.*, 92, 154–161, 2014.

1047 Salma, I., Németh, Z., Weidinger, T., Kovács, B., and Kristóf, G.: Measurement, growth types and
1048 shrinkage of newly formed aerosol particles at an urban research platform, *Atmos. Chem. Phys.*,
1049 16, 7837–7851, 2016a.

1050 Salma, I., Németh, Z., Kerminen, V. M., Aalto, P., Nieminen, T., Weidinger, T., Molnár, Á., Imre, K.,
1051 and Kulmala, M.: Regional effect on urban atmospheric nucleation, *Atmos. Chem. Phys.*, 16,
1052 8715–8728, 2016b.

1053 Salma, I., Varga, V., and Németh, Z.: Quantification of an atmospheric nucleation and growth process
1054 as a single source of aerosol particles in a city, *Atmos. Chem. Phys.*, 17, 15007–15017, 2017.

1055 Salma, I., Vasanits-Zsigrai, A., Machon, A., Varga, T., Major, I., Gergely, V., and Molnár, M.: Fossil
1056 fuel combustion, biomass burning and biogenic sources of fine carbonaceous aerosol in the
1057 Carpathian Basin, *Atmos. Chem. Phys.*, 20, 4295–4312, 2020a.

1058 Salma, I., Thén, W., Aalto, P., Kerminen, V.-M., Kern, A., Barcza, Z., Petäjä, T., and Kulmala, M.:
1059 Influence of vegetation on occurrence and time distributions of regional new aerosol particle
1060 formation and growth, *Atmos. Chem. Phys. Discuss.*, <https://doi.org/10.5194/acp-2020-862>, in
1061 review, 2020b.

1062 Shaman, J. and Kohn, M.: Absolute humidity modulates influenza survival, transmission, and
1063 seasonality. *Proc. Natl. Acad. Sci. USA*, 106, 3243–3248, 2009.

- 1064 Sussmann, R. and Rettinger, M.: Can we measure a COVID-19-related slowdown in atmospheric CO₂
1065 growth? Sensitivity of total carbon column observations, *Remote Sens.*, 12, 2387,
1066 <https://www.mdpi.com/2072-4292/12/15/2387>, 2020.
- 1067 Tobías, A., Carnerero, C., Reche, C., Massagué, J., Via, M., Minguillón, M. C., Alastuey, A., and
1068 Querol, X.: Changes in air quality during the lockdown in Barcelona (Spain) one month into the
1069 SARS-CoV-2 epidemic, *Sci. Total Environ.*, 726, 138540, 2020.
- 1070 VM 4, A levegőterheltségi szint határértékeiről és a helyhez kötött légszennyezőpontforrások
1071 kibocsátási határértékeiről (On the limit values of ambient air quality and emissions from fixed
1072 sources, in Hungarian), *Magyar Közlöny* 4, 487–533, 2011.
- 1073 Wang, P., Chen, K., Zhu, S., Wang, P., and Zhang, H.: Severe air pollution events not avoided by
1074 reduced anthropogenic activities during COVID-19 outbreak, *Resour. Conserv. Recycl.*, 158,
1075 104814, 2020.
- 1076 Warneck, P. and Williams, J.: *The Atmospheric Chemist's Companion, Numerical Data for Use in the*
1077 *Atmospheric Sciences*, Springer, Dordrecht, 2012.
- 1078 WHO (World Health Organization), Coronavirus disease 2019 (COVID-19): situation report, 51.
1079 World Health Organization, <https://apps.who.int/iris/handle/10665/331475>, last access 9 August
1080 2020.
- 1081 WMO (World Meteorological Organization), *Guide to Meteorological Instruments and Methods of*
1082 *Observation*, No. 8, Appendix 4B, Geneva, Switzerland, 2008.